Resource

Cell Reports

Analysis of the *S. pombe* Meiotic Proteome Reveals a Switch from Anabolic to Catabolic Processes and Extensive Post-transcriptional Regulation

Graphical Abstract

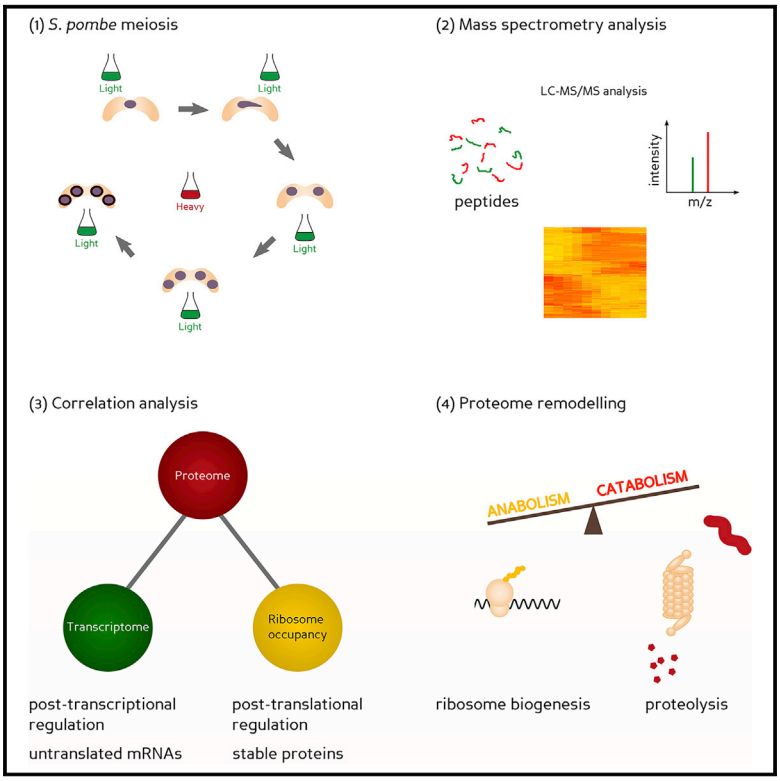

Highlights

- Quantification of 3,268 proteins throughout fission yeast meiosis
- High degree of post-transcriptional regulation of protein level during meiosis
- Global switch from anabolic to catabolic processes during meiosis
- Role of ESCRT-III complex in nuclear division and spore formation

Authors

Andrea Krapp, Romain Hamelin, Florence Armand, ..., Elena Cano, Marc Moniatte, Viesturs Simanis

Correspondence

viesturs.simanis@epfl.ch

In Brief

Krapp et al. study relative protein levels throughout *S. pombe* meiosis. Globally, there is a switch from catabolic to anabolic processes and extensive post-translational regulation. Some mRNAs persist, untranslated, after their protein decays during meiosis, while some stable proteins persist after the RNA decays.

Krapp et al., 2019, Cell Reports *26*, 1044–1058
January 22, 2019
https://doi.org/10.1016/j.celrep.2018.12.075

CellPress

OPEN ACCESS
CellPress

Cell Reports
Resource

Analysis of the *S. pombe* Meiotic Proteome Reveals a Switch from Anabolic to Catabolic Processes and Extensive Post-transcriptional Regulation

Andrea Krapp,[1] Romain Hamelin,[3] Florence Armand,[3] Diego Chiappe,[3] Lucien Krapp,[2] Elena Cano,[1] Marc Moniatte,[3] and Viesturs Simanis[1,4,*]

[1]EPFL SV ISREC UPSIM, SV2.1830, Station 19, 1015 Lausanne, Switzerland
[2]EPFL SV IBI-SV UPDALPE, AAB 1 17, Station 19, 1015 Lausanne, Switzerland
[3]EPFL Proteomics Core Facility, EPFL SV PTECH PTP, AI 0149, Station 15, 1015 Lausanne, Switzerland
[4]Lead Contact
*Correspondence: viesturs.simanis@epfl.ch
https://doi.org/10.1016/j.celrep.2018.12.075

SUMMARY

Meiotic progression in *S. pombe* is regulated by stage-specific gene expression and translation, changes in RNA stability, expression of anti-sense transcripts, and targeted proteolysis of regulatory proteins. We have used SILAC labeling to examine the relative levels of proteins in diploid *S. pombe* cells during meiosis. Among the 3,268 proteins quantified at all time points, the levels of 880 proteins changed at least 2-fold; the majority of proteins showed stepwise increases or decreases during the meiotic divisions, while some changed transiently. Overall, we observed reductions in proteins involved in anabolism and increases in proteins involved in catabolism. We also observed increases in the levels of proteins of the ESCRT-III complex and revealed a role for ESCRT-III components in chromosome segregation and spore formation. Correlation with studies of meiotic gene expression and ribosome occupancy reveals that many of the changes in steady-state protein levels are post-transcriptional.

INTRODUCTION

Schizosaccharomyces pombe is an excellent model for studying the basic processes of life (Fantes and Hoffman, 2016). Under conditions of nitrogen limitation, *S. pombe* cells of opposite mating type conjugate to form a diploid zygote. After pre-meiotic S phase, homologous chromosomes pair and recombine, while the nucleus undergoes an oscillatory "horsetail" movement (Chikashige et al., 1994; Robinow, 1977). A spindle is then formed, and an equational division (meiosis I) produces two nuclei, which undergo a reductional division (meiosis II), producing four haploid nuclei. Meiosis ends with the formation of ascospores. Spore formation initiates in meiosis II by the formation of the forespore membrane (FSM), a double membrane that emanates from the remodeled spindle pole body (SPB) and expands to encapsulate each nucleus (Ikemoto et al., 2000; Nakamura et al., 2008; Nakase et al., 2008). Expansion of the FSM is guided by Meu14p (Okuzaki et al., 2003) and the syntaxin Psy1p (Kashiwazaki et al., 2011; Maeda et al., 2009; Nakamura et al., 2001) and requires F-actin (Petersen et al., 1998; Yan and Balasubramanian, 2012) and the type I myosin Myo1p (Itadani et al., 2006). Ascospore formation is completed by deposition of spore wall material into the luminal space (reviewed by Shimoda, 2004) and requires the septation initiation network (SIN) (Krapp et al., 2006; Ohtaka et al., 2008; Pérez-Hidalgo et al., 2008; Yan et al., 2008).

Commitment to meiosis was reviewed recently (Yamashita et al., 2017). Briefly, nitrogen starvation of diploid *S. pombe* cells that are heterozygous at the *mat* locus results in large changes in the expression of protein-coding genes and non-coding RNAs (Bitton et al., 2011; Mata and Bähler, 2006; Mata et al., 2002, 2007). These include *mei3*, whose product inhibits the protein kinase Pat1p (Iino and Yamamoto, 1985; McLeod and Beach, 1988; McLeod et al., 1987; Nurse, 1985). This activates the RNA-binding protein Mei2p/meiRNA, which sequesters Mmi1p, allowing expression of early meiotic genes (Harigaya et al., 2006; Shichino et al., 2014; Yamanaka et al., 2010; Yamashita et al., 2012). Translational control (Duncan and Mata, 2014) and post-translational regulation of proteins are also important during meiosis. Macroautophagy (Mukaiyama et al., 2010) is required for entry into and progression through meiosis in fission yeast (Matsuhara and Yamamoto, 2016; Mukaiyama et al., 2009; Nakashima et al., 2006). Stage-specific protein degradation also plays an important role; for example, the meiosis-specific anaphase promoting complex (APC/C) inhibitor Mes1p prevents complete degradation of Cdc13p at the end of meiosis I (Izawa et al., 2005; Kimata et al., 2008), degradation of Sgo1p permits sister chromatid separation (Kitajima et al., 2004, 2006; Rabitsch et al., 2004; Riedel et al., 2006) and degradation of Hrs1p/Mcp6p allows formation of the meiosis I spindle (Funaya et al., 2012; Tanaka et al., 2005). Some SIN proteins are also degraded during meiosis (Krapp and Simanis, 2014).

In this study, we have analyzed changes in the *S. pombe* proteome during meiosis. Approximately 27% of the proteins analyzed show at least a 2-fold change in their relative level during meiosis. Our data reveal a significant remodeling of the proteostasis network during meiosis, with increases in proteins involved in catabolism and decreases in proteins involved in ribosome biogenesis. Comparison with published datasets of

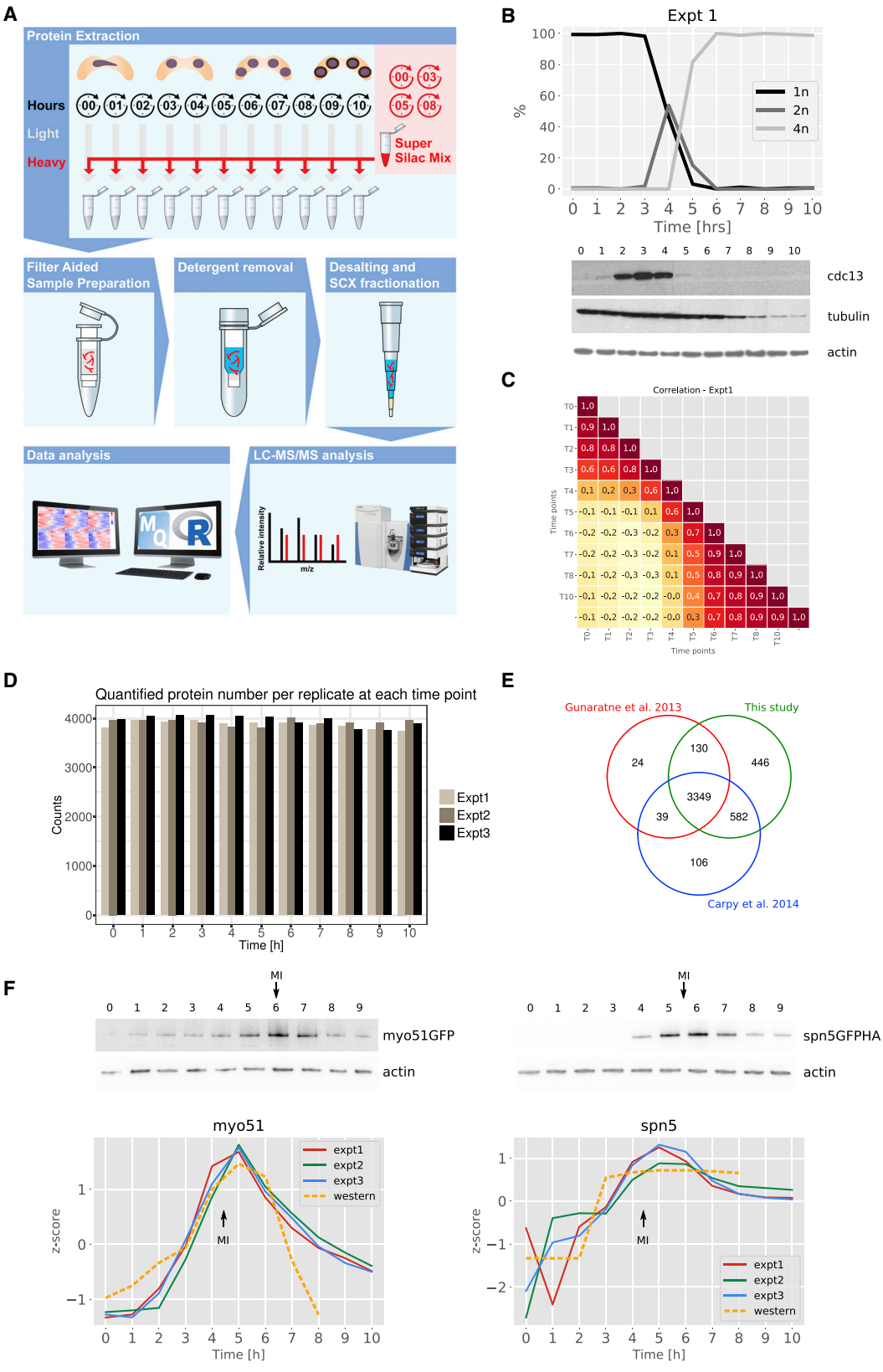

(legend on next page)

mRNA abundance and ribosome occupancy during meiosis reveals significant post-translational regulation of protein levels during meiosis.

RESULTS

Relative Quantification of the Proteome during Meiosis

To quantify changes in the proteome during *S. pombe* meiosis, relative protein levels were measured using synchronized cultures and stable isotope labeling with amino acids in cell culture (SILAC) (Ong et al., 2002). The temperature-sensitive mutant *pat1-114* (Iino and Yamamoto, 1985) was used to obtain good meiotic synchrony; this method also allows comparison with previous genome-wide studies of *S. pombe* meiosis (Bitton et al., 2011; Mata and Bähler, 2006; Mata et al., 2002, 2007).

Diploid *pat1-114* cells were accumulated in G1 by nitrogen starvation, and protein extracts were prepared after inactivation of Pat1p (Figure 1A). The data presented are from three independent biological replicates. Meiotic progression was followed by nuclear staining (Figures 1B and S1A). The cyclin Cdc13p (Figures 1B and S1A) accumulated at 2 hr during pre-meiotic S phase and disappeared at 4–5 hr, at the onset of the second meiotic division, as shown previously (Izawa et al., 2005). The steady-state level of alpha-tubulin (Figures 1B and S1A) decreases at 7–8 hr during spore formation, so actin was used as an internal control (Figure 2D). A super-SILAC standard (Geiger et al., 2010) was generated from labeled cells (Bicho et al., 2010; Carpy et al., 2015) using a pooled extracts from four time points; samples were processed as shown in Figure 1A.

In total, we quantified 4,507 proteins (≈89% of the proteome) with an average of 20.11 unique peptides per protein. The variation of protein coverage for each replicate was low (Figure 1D), and our quantitative protein measurements correspond well with previous *S. pombe* datasets (Carpy et al., 2014; Gunaratne et al., 2013): 3,349 proteins that were quantified in our dataset were also analyzed in these studies (Figure 1E); 446 proteins detected uniquely in this study were enriched in GO terms related to meiosis and spore formation ($p < 0.05$), as expected, because these studies used vegetatively growing cells (Table S5).

We quantified 3,101 proteins at every time point in all the replicates (Figure S1C). Data imputation of a single missing value using the mean of the flanking values was used to complete the data for an additional 167 proteins (Figure S1C, inset), giving a total of 3,268 proteins (Table S1). The average Pearson correlation coefficient between time points in pairs of replicates was 0.81, indicating a high degree of reproducibility (Figure S1D). Experiment 2 shows a slight delay both in the appearance of binucleate cells and the disappearance of Cdc13p compared with the other experiments (Figures 1B and S1A). Consistent with this, the mean of the correlation coefficients between experiments 1 and 3 is 0.85.

Extensive Proteome Remodeling during Meiotic Divisions

The mb.long function of the time course package in R Bioconductor allowed ranking of proteins on the basis of their T^2 statistics; 1,503 proteins, or 46% of the top T^2 ranked proteins ($T^2 > 135.62$), displayed significant changes in their levels compared with the null hypothesis of a flat profile (Murphy et al., 2015). The relative abundance of 880 of these proteins (≈27% of the proteome; Table S2) changed at least 2-fold during meiosis with a global transition point coinciding with the meiotic divisions (Figure 2A). To assess the temporal dynamics of protein abundance during meiosis, we calculated Pearson correlation coefficients for all pairs of time points. The relative protein levels were most highly correlated during early meiosis and during spore formation (Figures 1C and S1B). The steady-state level changes of several proteins in the dataset were confirmed by western blotting (Figures 1F and 2B), including Myo51p (Doyle et al., 2009), Spn5p (Onishi et al., 2010), For3p (Yan and Balasubramanian, 2012), Mei2p (Kitamura et al., 2001), and Cdc13p (Blanco et al., 2001). The relative protein levels measured here (Figure 2C) also correlated well with the published data for pat1-induced meiosis for Gas4p (de Medina-Redondo et al., 2008), Meu10p (Tougan et al., 2002), Meu14p (Okuzaki et al., 2003), Isp3p (Fukunishi et al., 2014), Spo5p (Kasama et al., 2006), Spo4p (Bitton et al., 2011; Nakamura et al., 2002), Mcp5p (Saito et al., 2006), and Spo15p (Ikemoto et al., 2000).

Temporal Correlation of mRNA and Relative Protein Levels Reveals Widespread Post-transcriptional Regulation

The extent to which regulation of the mRNA can explain changes in the protein levels was examined by comparing our dataset

Figure 1. Proteome Profiling during Meiosis in *S. pombe*

(A) Experimental design of total proteome analysis. Protein extracts prepared at the indicated time points from cells undergoing meiosis were mixed with pooled extracts from SILAC-labeled cells made at the indicated time points. After digestion, peptides were fractionated by cation exchange (SCX) and analyzed using liquid chromatography-tandem mass spectrometry (LC-MS/MS). The analysis was performed once for each biological replicate.

(B) Progression through meiosis was monitored by nuclear staining (DAPI) and plotted as the percentage of cells with one (1N), two (2N), or four (4N) nuclei (top). Bottom: western blot of protein extracts probed with an antibody to *S. pombe* Cdc13p; antibodies to actin and tubulin serve as internal controls. The result shown here is for experiment 1; the western blots and counting were performed once.

(C) Heatmap indicating the Pearson correlation coefficients of protein abundance between meiotic time points (T00–T10) for experiment 1.

(D) Histogram indicating the number of quantified proteins at each time point (0–10) for all three biological replicates.

(E) Venn diagram comparing the depth of protein coverage in three studies: "PeptideAtlas" (Gunaratne et al., 2013), absolute *S. pombe* proteome (Carpy et al., 2014), and this study.

(F) Validation of SILAC-quantified relative protein abundance by western blotting. Protein extracts of strains expressing chromosomally tagged Myo51p-GFP (left) or Spn5p-GFP-HA (right) fusion proteins were prepared at the indicated times following *pat1-114* inactivation: the western blot was probed with anti-GFP antibody or antibody to actin as control. The change in relative protein abundance (Z score) is shown below for each biological replicate. The broken orange line represents quantification of the chemiluminescence signals from the western blot, normalized to that of the actin control. The midpoint of meiosis I is indicated above the western blot. Each western blot shown was performed once, when the optimum antibody concentration had been established.

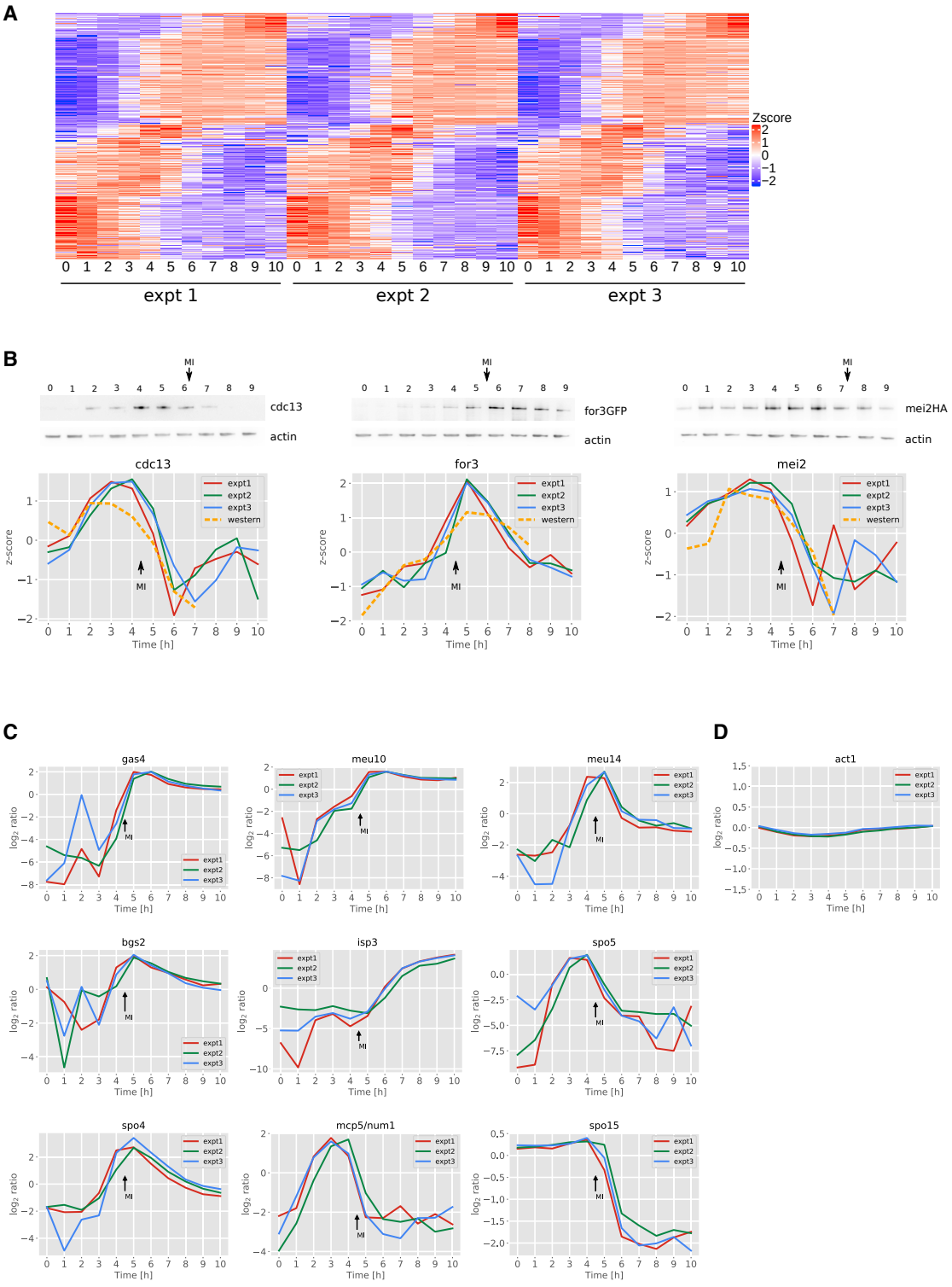

Figure 2. Validation of Selected Proteins

(A) Aligned heatmaps of the meiotic time course profiles (0–10) from the three biological replicates. The 880 proteins that varied significantly (T^2 [Hotelling test] and >2-fold difference in at least one time point) were $\log_2$-transformed and Z score-normalized. The x axis is time (hours).

(B) Validation of SILAC-quantified relative protein abundance by western blotting. Protein extracts from wild-type (left) or strains expressing chromosomally tagged For3p-3GFP (middle) or Mei2p-HA (right) fusion proteins were prepared at the indicated times after *pat1-114* inactivation. A western blot was probed with

(legend continued on next page)

with the meiotic transcriptome (Mata et al., 2002). Calculating the pairwise Pearson correlation coefficients for all pairs of time points in the meiotic mRNA time course revealed that significant changes in the mRNA already occur during the early stages of meiosis, in contrast to the variations in protein levels (Figure S1E). This partly explains the broad distribution observed in the histogram plot of the pairwise RNA/protein Pearson correlation coefficients (Figure 3A; mean Pearson correlation coefficient = 0.24). Some mRNA-protein pairs show good correlations, whereas others show no correlation or even negative correlations (Figure 3B), suggesting widespread post-transcriptional regulation, consistent with previous studies (Duncan and Mata, 2014; Liu et al., 2016).

To discriminate between transcriptional and post-transcriptional regulation, mRNA-protein pairs were subdivided into three groups by k-means clustering of the relative distance between mRNA and protein levels (Table S3; Figure 3C; no additional groups were found using $k > 3$). Group 1 contains genes showing good correlations between mRNA and protein levels, indicating gene regulation mainly at the transcriptional level. The annotation tool STRING (Szklarczyk et al., 2015) was used to assign enriched GO (Gene Ontology) terms. We found that this group comprises, among others, proteins playing a role in spore formation, which are expressed specifically during meiosis (Table S6).

Group 2 comprises mRNA-protein pairs whose relative distance increases during meiosis, resulting mainly from a combination of a decrease in protein level accompanied by an increase in the mRNA level. A profile of this type is consistent with post-transcriptional regulation of protein level, either inhibition of translation, protein degradation or a combination thereof, leading to an accumulation of non-translated mRNAs. GO term enrichment analysis reveals proteins involved mainly in the generation of ribosomes and mature RNAs (Table S5).

Group 3 contains proteins whose levels increase while the mRNA level decreases, suggesting that the protein product is either long lived or efficiently translated. The biological process (BP) term enrichment reveals an enrichment for protein catabolism (with GO terms including APC/C and proteasome), protein transport (with GO term enrichment for endosomes, COPI/II coated vesicles, exocyst, and Golgi apparatus), cell cycle regulators, and chromosome organization (Table S5). These may reflect the extensive remodeling that occurs late in meiosis to produce spores.

Overall, this analysis points toward a global adaptation of the cell as it makes the transition to a dormant state as a spore, through an upregulation of catabolic pathways (allowing a rapid modification of the protein content), concomitant with a global downregulation of the anabolic pathways. Our data suggest that a significant part of these changes arise via post-transcriptional regulation.

Temporal Correlation of Ribosome Occupancy and Relative Protein Levels Highlights Post-translational Regulation during Meiosis

To assess the contribution of translation or post-translational regulation, we performed a correlation analysis with the meiotic ribosome occupancy (RO) dataset (Duncan and Mata, 2014). A broad distribution in the plot of the pairwise Pearson correlation coefficients (Figure 3D), with a mean Pearson correlation coefficient of 0.24, is consistent with a high degree of post-translational regulation. We used k-means clustering to partition the RO-protein pairs using the relative distance between RO and protein levels (Table S4; Figure 5A). Only two groups, named A and B, were identified ($k > 2$ did not reveal any additional profiles). Group A comprises genes showing a good correlation between RO and protein levels, indicating that protein levels and translation rates vary similarly during meiosis; this group is enriched in proteins involved in ribosome biogenesis, translation, and actin cytoskeleton (Table S5). Group B comprises proteins whose levels increased while the RO of the mRNA decreased during meiotic progression. This group is likely to be enriched in stable proteins. GO term analysis reveals an enrichment for protein catabolic processes (Table S5). We failed to detect any group that displayed an increase in the RO-protein distance during the time course of meiosis. These mRNAs would have been highly translated but giving rise to proteins that are rapidly degraded. We conclude that this method of regulation is not widely used among the proteins we have analyzed.

The mRNA-protein correlation analysis indicates that some mRNAs accumulate during the late stages of meiosis. Cross-correlation shows that the RO-protein pairs having Pearson correlations greater than 0.4 (n = 1,318) mainly show also good correlations for the mRNA-protein pair (Figure 5B). However, a significant number of the well-correlated RO-protein pairs (n = 441 [33%]) show increases in relative mRNA levels, whereas the relative protein level decreases during meiosis (Figure 5B, group 2), consistent with the accumulation of non-translated mRNAs. GO term analysis reveals that they are mainly genes involved in the ribosome biogenesis and coding for ribosomal proteins (Table S5).

Temporal Dynamics of Relative Protein Levels during Meiosis

Next, we used a template matching strategy to define temporal patterns among the 880 significantly varying proteins. Six clusters were specified as follows: clusters 1 and 2 show a stepwise increase before meiosis I and at the end of meiosis II, respectively; clusters 5 and 6 show a stepwise decline before meiosis I and the end of meiosis II, respectively; and clusters 3 and 4 show transient peaks corresponding to the meiosis I-II transition and S-phase/recombination/horsetail stage, respectively (Figure 4, black lines).

antibody to Cdc13p, anti-GFP, or anti-HA antibodies; an antibody to actin was used as control. The Z score of the relative changes in abundance are shown below for each biological replicate and the western blot. The midpoint of meiosis I is indicated above the western blot. The broken orange line represents quantification of the chemiluminescence signal from the western blot, normalized to that of the actin control. Each western blot shown was performed once, when the optimum antibody concentration had been established.

(C) Plot of the $\log_2$ relative levels for each biological replicate of proteins whose steady-state level is known to vary through meiosis.

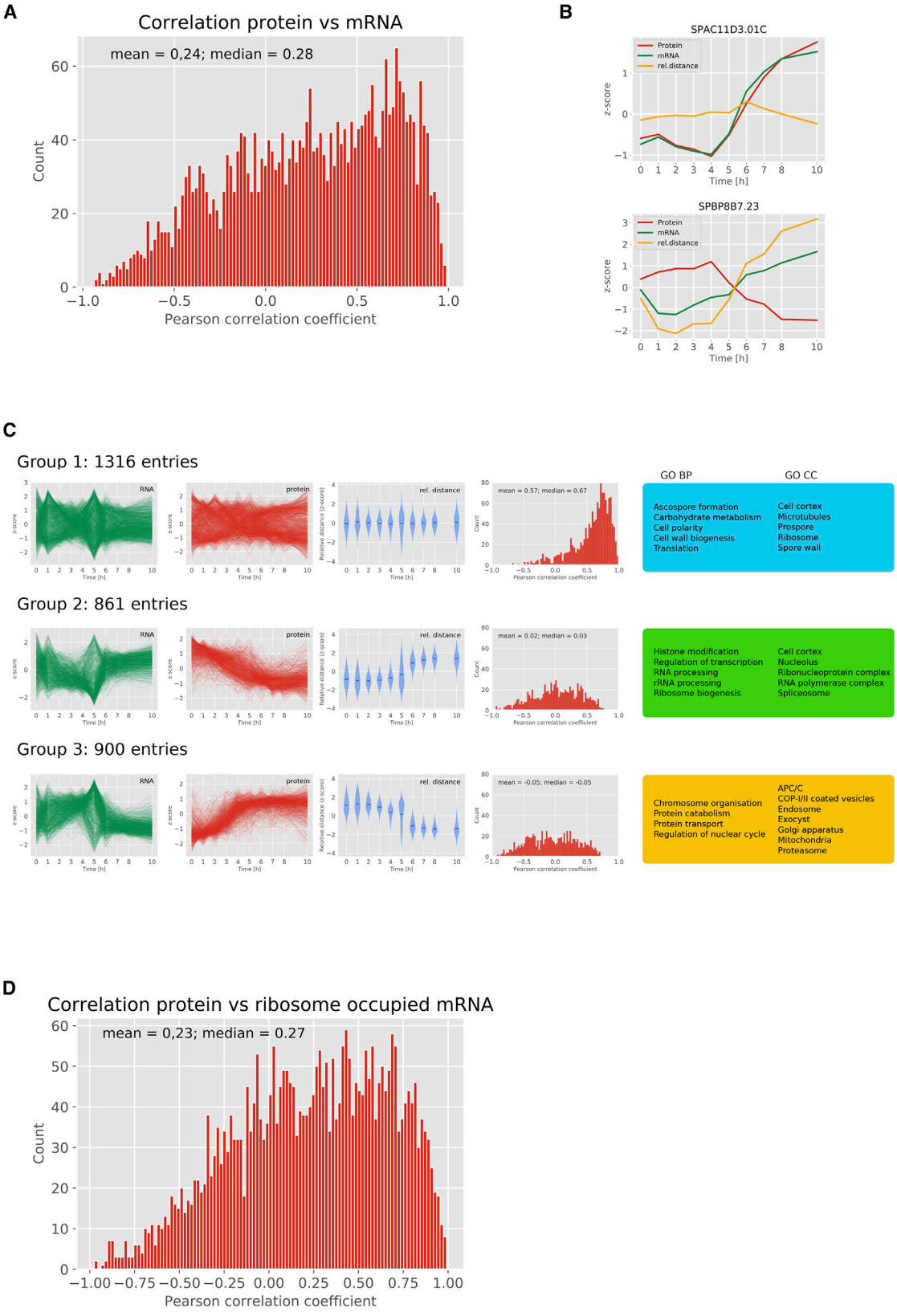

(legend on next page)

The summed Euclidean distance was calculated between a protein's profile and each of the six templates at every time point. The proteins were assigned to the cluster giving the smallest total Euclidean distance (Table S2). Eight hundred sixty-seven of the 880 proteins were assigned to one of the six clusters; the four clusters showing a stepwise alteration in protein level account for 786 (≈91%) of these.

Proteins in cluster 1 play a function in spore formation and in protein catabolism, which is necessary to complete the meiotic divisions. Clusters 3 and 4 showed GO term enrichment for BPs such as meiosis and DNA repair and cellular components such as condensed chromosome. By contrast, expression of ribosomal proteins decreases at the onset of meiotic divisions (cluster 5), which correlates with the decrease in protein translation efficiency observed after induction of meiosis (Duncan and Mata, 2014). There is also a decrease in enzymes involved in synthesis of the cell wall. These changes may reflect the transition to a quiescent state. Proteins whose levels decrease after the meiotic divisions include cytoskeletal proteins (actin and microtubule cytoskeletons; cluster 6), and those involved in cell proliferation, which is consistent with the cell having completed the two meiotic divisions. Cluster 2 did not show any specific enrichment for GO terms. Overall, the mean Pearson correlation coefficients between mRNA or RO and protein levels during meiosis for the proteins in the six clusters increased to 0.39 for mRNA and 0.43 for RO. Clusters 2 and 3 showed the highest overall correlation between mRNA and protein, suggesting that transcriptional control plays an important part in regulating these genes (Figure 4). Clusters 5 and 6 show good correlations between protein and RO, though the correlation with mRNA level was poor.

There are three waves of gene expression controlled by transcription factor cascades during meiosis (Mata et al., 2002, 2007). First, Rep1p activates expression of genes involved in pre-meiotic S phase. After homologous recombination, Mei4p activates transcription of genes important for meiotic nuclear divisions and early steps of spore formation. Finally, late-phase genes, whose products are required for spore maturation, are activated by a combination of Atf21p and Atf31p. The Pearson correlation coefficients for mRNA-protein pairs for the targets of these meiotic transcription factors revealed a positive trend in all the cases with a mean Pearson correlation coefficient of approximately 0.45 (Figure 5C). A good correlation (mean Pearson correlation coefficient = 0.604) was also observed for the meiotically upregulated (*mug*) genes (Martín-Castellanos et al., 2005). The *mug* genes were assigned mainly to either cluster 1 and 2 (Figure 5D; Table S6). The majority of targets of the early meiosis-specific transcription factor Rep1p were assigned to cluster 4, which peaks during the horsetail stage (pre-meiotic S phase and recombination). Most Mei4p target gene products belong to cluster 1, while the Atf21p/Atf22p targets were found mostly in cluster 2. Therefore, the relative level of the proteins expressed from genes that are targets of the major meiosis-specific transcription factors generally reflect the mRNA level.

Meiosis-Specific Changes in Proteostatic Networks

The relative levels of proteins implicated in two branches of the proteostatic control, namely, protein synthesis and protein degradation (Klaips et al., 2018), change in opposite direction during meiosis. We observed decreases in the levels of proteins that play a role in ribosome biogenesis (GO: 0042254). Concomitantly, we observed an increase in proteins implicated in proteolysis (GO: 0006508), which is required for meiotic progression and may also eliminate excess or damaged proteins (Figure 6A). In addition to proteins involved in autophagy, these included components of the APC/C and the proteasome. The level of all the subunits of the APC/C (7 of 13), and the proteasome (36 of 38; Figure 6B) present in our dataset increased as cells progressed through meiosis. Of the 25 proteins involved in autophagy, the levels of 13 increased, while 3 did not vary; a further 9 were not quantified at all time points (Table S7).

The ESCRT-III Complex Is Required for Faithful Spore Formation

The relative protein levels of the six members of the ESCRT-III complex, namely, Cmp7p, Did2p, Did4p, Vps20p, Vps24p, and Vps32p, all increased at the onset of meiotic divisions (Figure 6C). The levels of the two components of ESCRT-0, Hse1p and Sst4p, increased <2-fold during meiosis. The ESCRT-1 protein Sst6p did not change significantly during meiosis, while Vps28p is not in our dataset. None of the three *S. pombe* ESCRT-II proteins, Dot2p, Vps25p, and Vps36p, were quantified in this study.

Previous studies have shown that mutation of some ESCRT components (the ESCRT-0 component Vps27p/Sst4p, the ESCRT-III components Vps20p and Vps32p and their associated proteins Vps4p and Sst2p, and the ESCRT-I protein Sst6p) affect meiosis, reducing the number of asci with four

Figure 3. Correlation of the Proteome Time Course Dataset with Meiotic mRNA and Ribosome Occupancy Datasets

(A) Histogram showing the distribution of Pearson correlation coefficients for a comparison of the dataset obtained in this study, with that of Mata et al. (2002), for each mRNA-protein pair. The mean and median Pearson correlation coefficient for this analysis is shown.

(B) Examples of two proteins showing a strongly positive (SPAC11D3.01c) or a strongly negative (SPBP8B7.23) correlation between the mRNA and the protein profiles. Plots of the Z score-normalized levels of the protein (red), mRNA (green), or relative distance (mRNA level − protein level, see text; yellow) during the meiotic time course.

(C) The plots show the results of clustering using Mini-batch k-means, of the relative distance between Z score-normalized mRNA and protein levels for the three groups discussed in the text. The plots show the Z score (ordinate) for mRNA levels (green) and protein levels (red). The relative distance (blue) is presented as a violin plot (ordinate) against time (abscissa). The histograms show the distribution of Pearson correlation coefficients for each mRNA-protein pair in each group. The number of proteins and the mean and median of the Pearson correlation coefficients in each group are indicated. The proteins in each cluster were tested for enrichment of Gene Ontology, biological process terms (GO BP; left) and GO, cellular component terms (GO CC; right) using STRING.

(D) Histogram showing the distribution of Pearson correlation coefficients for each ribosome-protein pair, comparing our dataset with that of Duncan and Mata (2014). The mean and median of the Pearson correlation coefficient for this analysis are shown.

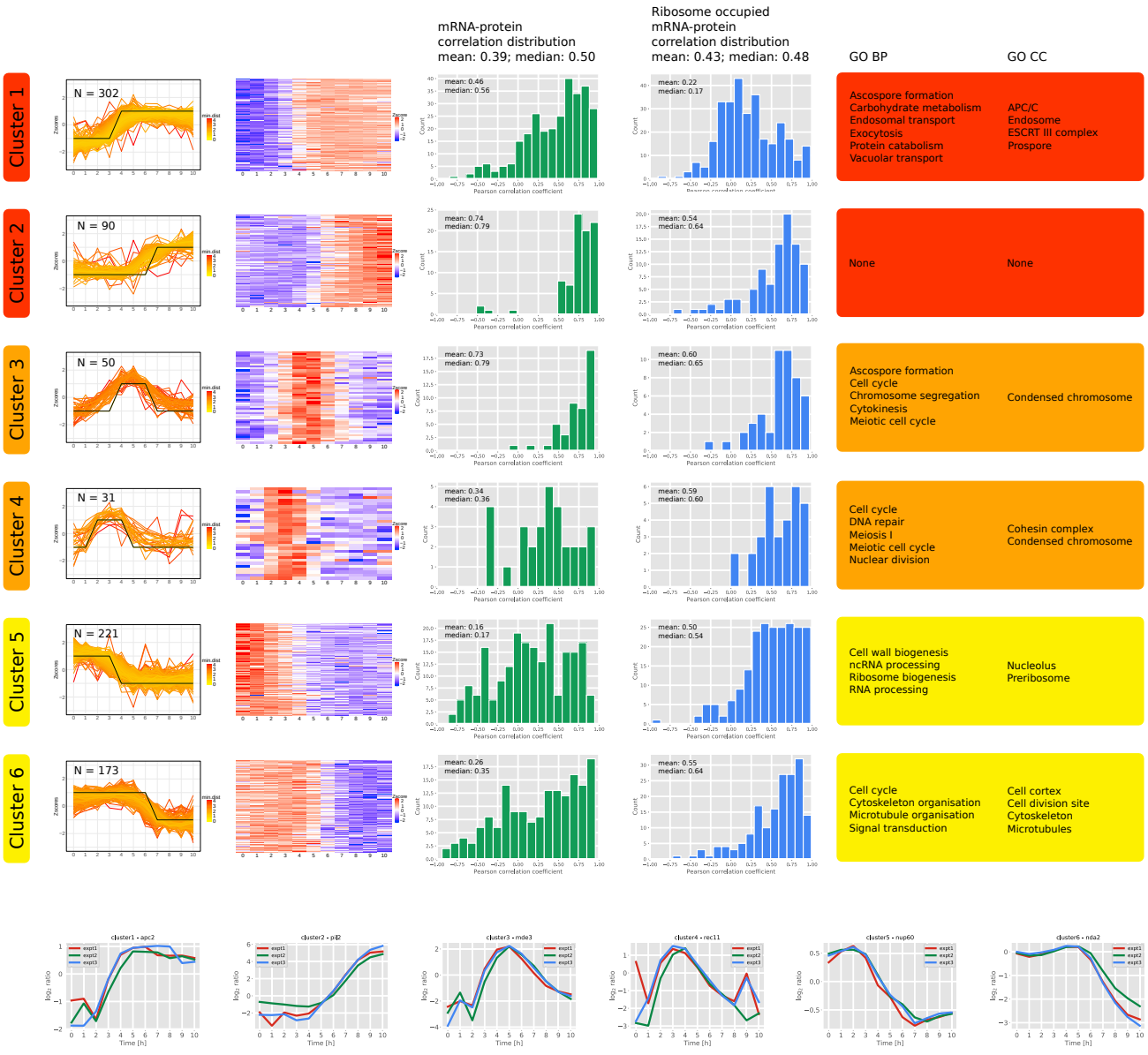

Figure 4. Comprehensive Temporal Protein Clustering

The plots show the following parameters for the six clusters of the proteins that vary significantly during the time course, from left to right: (1) Plot of the Z score-normalized protein levels in heatmap colors according to the distance to the template profile (in black), plotted against time. The number of proteins in the cluster is indicated. (2) Heatmap of the time course Z score-normalized levels, plotted against time. (3) Histogram of the distribution of Pearson correlation coefficients for mRNA-protein pairs. The mean and median of the Pearson correlation coefficients are indicated. (4) Histogram of the distribution of Pearson correlation coefficients for ribosome-protein pairs. The mean and median of the Pearson correlation coefficients are indicated. (5) GO BP (left) and GO CC (right) terms enriched in the cluster (see STAR Methods). The plots at the bottom of the figure show a representative example from each cluster.

spores and affecting spore morphology (Onishi et al., 2007). Furthermore, a genome-wide screen revealed that mutation of the ESCRT-III component Cmp7p and ESCRT-II component Vps25p produced a significant increase in the number of aberrant asci (Blyth et al., 2018). These findings, and the concerted increase in ESCRT-III proteins, prompted us to investigate whether other components of the ESCRT-III complex play a role during meiosis. Homozygous matings of null alleles of the *cmp7*, *did2*, *did4*, *vps20*, and *vps24* genes were analyzed for effects upon spore formation and DNA segregation. With the exception of *vps24*, deletion of any of these genes resulted in the formation of a significant number of aberrant asci, confirming the previous analyses of *vps20-Δ* and *cmp7-Δ*, cited above. A preponderant phenotype was that asci contained fewer than four spores (Figure 6D), indicating a defect in spore formation. Furthermore, we observed asci containing more, or fewer, than

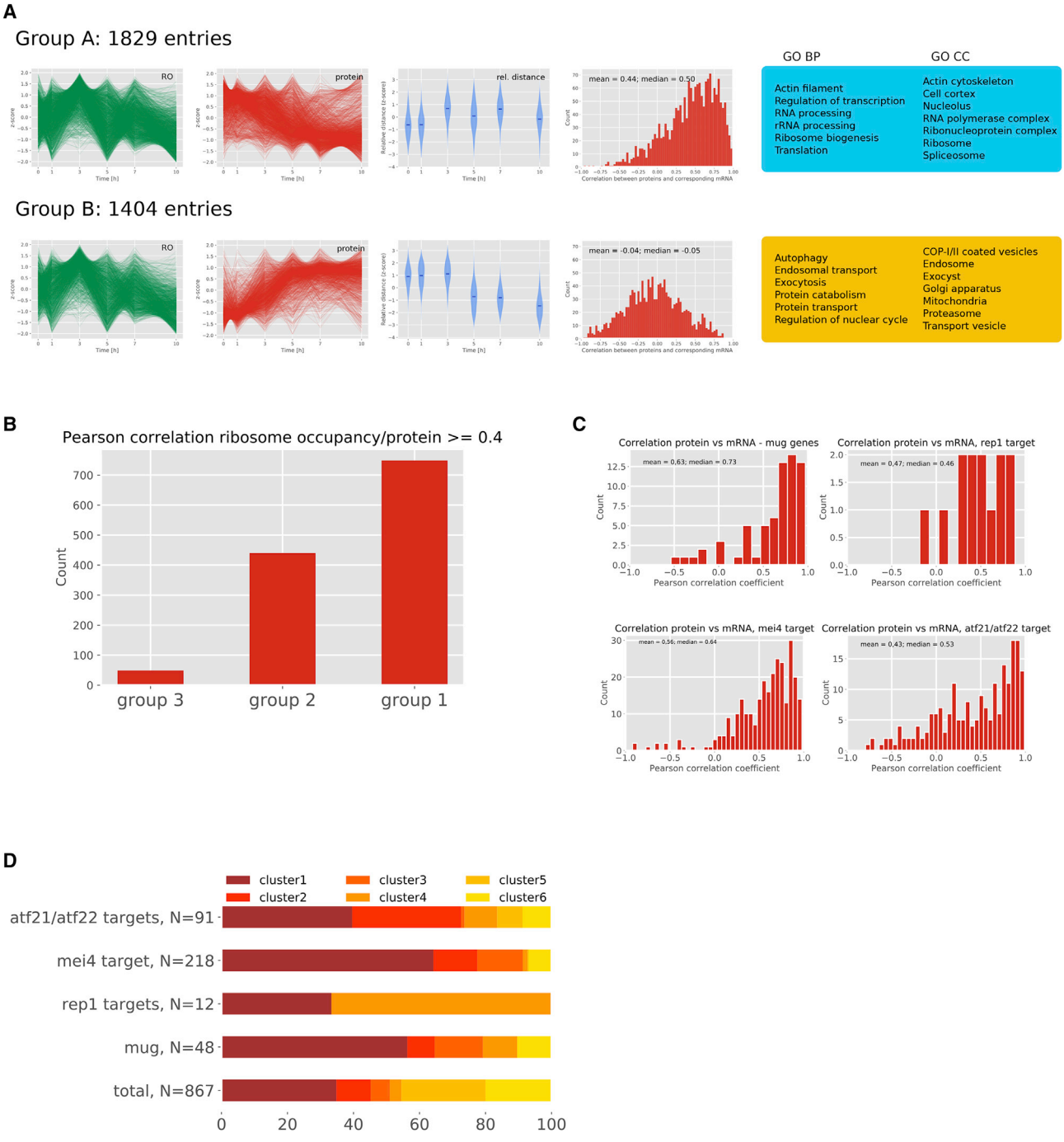

Figure 5. Correlation of the Proteome Time Course Dataset with Meiotic mRNA and Ribosome Occupancy Datasets

(A) Clustering of relative distance between Z score-normalized ribosome occupancy and protein levels using Mini-batch k-means. Plots of the Z score for ribosome occupancy (RO) levels (green), relative protein levels (protein; red), and the relative distance (rel. distance; blue) are shown as a violin plot. The histograms showing the distribution of Pearson correlation coefficients for each mRNA-protein pair are shown for each group. The number of proteins and the mean and median of Pearson correlation coefficients of each group are indicated. The proteins in each cluster were tested for enrichment of GO BP (left) and GO CC (right) using STRING; the enriched terms are listed.

(B) The histogram shows a plot of the number of ribosome-protein pairs in the entire dataset that show a good correlation (Pearson correlation coefficients $\geq$ 0.4; 1,318 entries), which fall into one of the three mRNA-protein correlation clusters shown in Figure 3C (group 1, mRNA = protein; group 2, mRNA > protein; group 3, protein > mRNA).

(legend continued on next page)

four DNA foci, consistent with mis-segregation of chromosomes during meiosis (Figures 6D and 6F). Because aneuploid *S. pombe* cells grow very poorly (Niwa and Yanagida, 1985), errors in chromosome segregation in meiosis should manifest as a decrease in spore viability. The viability of spores resulting from homozygous matings of null alleles of *cmp7*, *did2*, *did4*, and *vps20* was significantly reduced (Figure 6E). A *did4*-null mutant in *S. cerevisiae* also reduces sporulation efficiency and viability (Deutschbauer et al., 2002). Future studies will address the nature of the defects that produce these phenotypes.

DISCUSSION

We have used a super-SILAC labeling approach to study the relative levels of proteins during *S. pombe* meiosis. We detected 89% of the predicted proteome and quantified 3268 proteins (≈66% of the proteome). The levels of 27% of these proteins changes by at least 2-fold at some stage in meiosis. These proteins were subdivided into six clusters using a template-matching strategy. Two clusters show peaks either during pre-meiotic S phase/recombination or the meiotic divisions. The remainder show step changes during either pre-meiotic S phase/recombination or the meiotic divisions.

Globally, our analysis reveals a switch from anabolic to catabolic processes as meiosis proceeds. The increase in protein degradation activity is consistent with the need to generate building blocks for spore formation in a nutrient-poor environment. Specific degradation by the APC/C is essential in both meiosis I and meiosis II (Blanco et al., 2001; Chikashige et al., 2017; Izawa et al., 2005). Because the levels of both the APC/C and proteasome remain high after completion of meiosis II, it may be that they play a role in the final steps of meiosis, such as spore maturation. It is noteworthy that during meiosis II, the proteasome subunit Pad1p relocalizes to a region between the two dividing nuclei where the FSMs close and is seen as punctate dots at the nuclear periphery in spores (Wilkinson et al., 1998). Analysis of the meiotic proteome in *S. cerevisiae* has revealed a similar upregulation of catabolic pathways (Becker et al., 2017; Wen et al., 2016), suggesting that a generalized increase in protein degradation capacity may be a common feature in meiosis, at least in fungi.

Analysis of the correlation between mRNA levels, RO, and protein levels during meiotic progression reveals positive correlations for only a subset of genes. These are enriched for the targets of meiosis-specific transcription factors. It is striking that a significant fraction of mRNA-protein pairs show anti-correlation; that is, the relative level of protein decreases while the mRNA remains high, or vice versa. One noteworthy group of genes in the former category are those for ribosomal proteins, which may presage the quiescent state of the spore. The persistence of the mRNA may also point to some of it being stored in the spore. Previous studies have shown that during spore germination in *S. cerevisiae*, protein synthesis starts rapidly, before RNA transcription (Xu and West, 1992), and that spores contain mRNA available for translation, which may help maintain the viability of the spore (Brengues et al., 2002). In this context it is noteworthy that Mmi1p not only targets some mRNAs for destruction but also sequesters others in nuclear foci, inhibiting their translation (Shichino et al., 2018). Storing a subset of mRNA for cellular components that are essential for manufacture of ribosomes may be a mechanism to facilitate the germination of the spore and its transition to a vegetative cell. Future studies will investigate whether this is the case in *S. pombe*.

Studies in *S. cerevisiae* revealed widespread changes in the translation efficiency of genes during meiosis, which was attributed in large part to the use of microORFs (Brar et al., 2012). Extending this, a recent study of *S. cerevisiae* meiosis has highlighted changes in the 5′ UTR of mRNAs as a regulatory mechanism; switching to an alternative 5′ UTR decreases the efficiency of translation initiation, which maintains mRNA levels while decreasing those of the protein (Cheng et al., 2018). To address whether such a mechanism is also widespread in *S. pombe* meiosis, we examined orthologs of the genes identified by Cheng et al. (2018), which show a poor mRNA-protein correlation and contain an upstream AUG in an alternative 5′ UTR. Our dataset contains 285 of the 462 orthologs of this gene set. A plot of the correlation coefficients between mRNA and protein levels did not show an enrichment for anti-correlation in this group of genes (mean Pearson correlation coefficient = 0.18; not shown), suggesting that this regulatory mechanism may not apply widely in *S. pombe*. The analysis of RO during meiosis in *S. pombe* also supports this view, because it did not detect any increase in the use of micro-ORFs during meiosis (Duncan and Mata, 2014). Furthermore, if we analyze those genes that have an ATG in the 5′ UTR, either in the group of genes mentioned above, or the whole dataset, we do not find any enrichment for anti-correlation between mRNA and protein levels. However, it should be noted that the mapping of *S. pombe* 5′ UTRs in meiosis has not been published to date, and the analyses discussed above use 5′ UTRs mapped in vegetatively growing cells.

Our dataset has revealed that the relative levels of all the subunits of the ESCRT-III complex increase during meiosis. Analysis of meiosis in null mutants of ESCRT-III subunits whose protein levels increases revealed that four of five mutants show aberrant meiotic progression and/or spore formation. Previous studies have implicated the ESCRT-III components Vps20p, Vps32p, and Cmp7p in the execution of a faithful meiosis and spore formation (Blyth et al., 2018; Onishi et al., 2007), consistent with the observations in this study. As a membrane remodeling complex, the ESCRT-III proteins play a role in a variety of cellular pathways, including endosomal maturation (Hurley and Emr, 2006), multi-vesicular body formation (Liu et al., 2015), membrane fission during the abscission step of cytokinesis (Carlton and Martin-Serrano, 2007; Morita et al., 2007), and centrosome

(C) Histograms showing the distribution of Pearson correlation coefficients for specific mRNA-protein pairs. Upper left: meiotically upregulated (mug) genes (n = 66); upper right: Rep1p transcription factor targets (n = 13): lower left: Mei4p transcription factor targets (n = 286); lower left: Atf21p/Atf22p transcription factor targets (n = 206). The mean and median Pearson correlation coefficients for each group are indicated.
(D) Distribution in percentage of all (total), meiotically upregulated (mug), Rep1p, Mei4p, or Atf21p/Atf22p target genes to protein clusters 1–6.

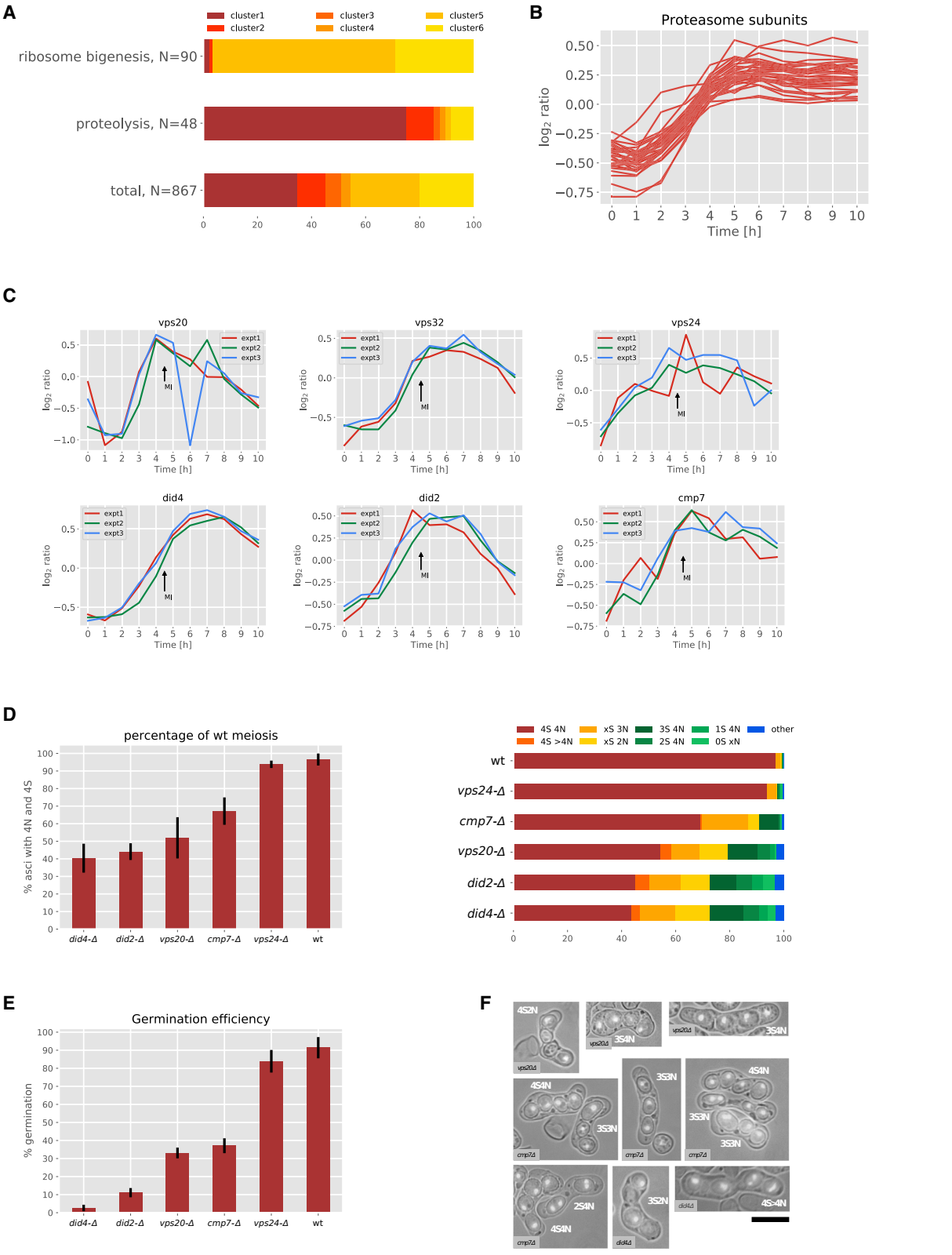

(legend on next page)

dynamics (Morita et al., 2010). In *S. pombe*, the ESCRT-III complex has been shown to be important for cytokinesis and cell separation (Bhutta et al., 2014), as well as in SPB insertion into the nuclear membrane in mitosis (Frost et al., 2012; Gu et al., 2017). It is noteworthy that deletion of the ESCRT-II subunit Dot2p leads to overamplification of SPBs during meiosis in *S. pombe* (Jin et al., 2005). A similar role in meiosis could produce the observed phenotypes. Moreover, proteins of the ESCRT-0, I, II, and III complexes also mediate selective autophagy in *S. pombe* (Liu et al., 2015). The collective upregulation of ESCRT-III proteins in meiosis may therefore indicate a role for them in the switch to catabolism that occurs during meiosis. A decreased ability to recycle cellular components for meiosis and spore formation under starvation conditions may also contribute to the multiple meiotic defects we observe. Future studies will examine the role of ESCRT-III proteins in meiosis in *S. pombe*.

STAR★METHODS

Detailed methods are provided in the online version of this paper and include the following:

- KEY RESOURCES TABLE
- CONTACT FOR REAGENT AND RESOURCE SHARING
- EXPERIMENTAL MODEL AND SUBJECT DETAILS
  - Yeast methods
  - List of main yeast strains used
  - Meiotic synchronization
  - SILAC labeling
- METHOD DETAILS
  - Sample processing for mass spectrometry
  - Liquid chromatography and MS
  - Protein extraction
  - Data validation by western blotting
  - DAPI staining
  - Spore formation and germination efficiency assays
- QUANTIFICATION AND STATISTICAL ANALYSIS
  - Computational Proteomics
  - Bioinformatic, statistical analysis and clustering
  - Correlation analysis
- DATA AND SOFTWARE AVAILABILITY

SUPPLEMENTAL INFORMATION

Supplemental Information includes one figure and nine tables and can be found with this article online at https://doi.org/10.1016/j.celrep.2018.12.075.

ACKNOWLEDGMENTS

We thank Iain Hagan (Manchester, UK) for sharing the improved SILAC labeling protocol before publication. We thank Sophie Martin (Lausanne, Switzerland), Iain Hagan (Manchester, UK), and Takashi Toda (Hiroshima, Japan) for strains; Keith Gull (Oxford, UK) for TAT-1; and Thierry Duperrut for drawing Figure 1A. We thank the Swiss National Science Foundation for funding (grant number SNF 31003A 156769/1) and École polytechnique fédérale de Lausanne (EPFL) for core support.

AUTHOR CONTRIBUTIONS

A.K. and V.S. conceived the biological experiments. Most were performed by A.K., and some were done by V.S., with technical assistance from E.C. Mass spectrometry analysis was designed by M.M., D.C., and R.H. and performed by R.H. and D.C. Data analysis was performed by F.A., A.K., and L.K. The paper was written by A.K. and V.S.; all authors were given the opportunity to comment.

DECLARATION OF INTERESTS

The authors declare no conflicting interests.

Received: July 19, 2018
Revised: November 9, 2018
Accepted: December 17, 2018
Published: January 22, 2019

REFERENCES

Becker, E., Com, E., Lavigne, R., Guilleux, M.H., Evrard, B., Pineau, C., and Primig, M. (2017). The protein expression landscape of mitosis and meiosis in diploid budding yeast. J. Proteomics *156*, 5–19.

Bhutta, M.S., Roy, B., Gould, G.W., and McInerny, C.J. (2014). A complex network of interactions between mitotic kinases, phosphatases and ESCRT proteins regulates septation and membrane trafficking in S. pombe. PLoS ONE *9*, e111789.

Bicho, C.C., de Lima Alves, F., Chen, Z.A., Rappsilber, J., and Sawin, K.E. (2010). A genetic engineering solution to the "arginine conversion problem" in stable isotope labeling by amino acids in cell culture (SILAC). Mol. Cell. Proteomics *9*, 1567–1577.

Figure 6. Changes in the Proteostasis Network and Role of ESCRT-III Complex during Meiosis

(A) Distribution in percentage of all (total), or functional categories GO BP ribosome biogenesis (GO: 0042254) and GO BP proteolysis (GO: 0006508) to protein clusters 1–6.

(B) Plot of the $\log_2$ relative levels (mean of the three biological replicates) for the proteasome subunits.

(C) Plot of the $\log_2$ relative levels for each biological replicate of ESCRT-III complex proteins.

(D) Histogram showing the percentage of asci containing four nuclei and four spores for wild-type and ESCRT-III deletions strains is shown on the left. The error bars in the left-hand plot indicate SD. The frequencies of the different phenotypes observed for each of the null mutant strains, and a wild-type control, is shown on the right. The abbreviations correspond to four spores and four nuclei (4S 4N), four spores and more than four nuclei (4S > 4N), three nuclei (xS 3N), two nuclei (xS 2N), three spores and four nuclei (3S 4N), two spores and four nuclei (2S 4N), one spore and four nuclei (1S 4N), no spores (0S xN), and others. The data presented are the mean of three independent experiments. The number of asci examined is shown in Table S9.

(E) A plot of the percentage spore viability of spores arising from self-mating of the indicated null mutant strains and a wild-type control. The error bars indicate the SD of three experiments. The germination efficiency is calculated as the percentage of spores giving rise to a colony. The number of spores examined is shown in Table S9.

(F) Illustrations of the observed abnormal sporulation phenotypes. Cells were processed as in (D) and phenotypes are annotated as described in (D). The gene that has been deleted in the displayed cells is indicated on the light gray square. These are representative images, drawn from all three biological replicates. The scale bar represents 10 μm.

Bitton, D.A., Grallert, A., Scutt, P.J., Yates, T., Li, Y., Bradford, J.R., Hey, Y., Pepper, S.D., Hagan, I.M., and Miller, C.J. (2011). Programmed fluctuations in sense/antisense transcript ratios drive sexual differentiation in S. pombe. Mol. Syst. Biol. *7*, 559.

Blanco, M.A., Pelloquin, L., and Moreno, S. (2001). Fission yeast mfr1 activates APC and coordinates meiotic nuclear division with sporulation. J. Cell Sci. *114*, 2135–2143.

Blyth, J., Makrantoni, V., Barton, R.E., Spanos, C., Rappsilber, J., and Marston, A.L. (2018). Genes important for *Schizosaccharomyces pombe* meiosis identified through a functional genomics screen. Genetics *208*, 589–603.

Brar, G.A., Yassour, M., Friedman, N., Regev, A., Ingolia, N.T., and Weissman, J.S. (2012). High-resolution view of the yeast meiotic program revealed by ribosome profiling. Science *335*, 552–557.

Brengues, M., Pintard, L., and Lapeyre, B. (2002). mRNA decay is rapidly induced after spore germination of Saccharomyces cerevisiae. J. Biol. Chem. *277*, 40505–40512.

Carlton, J.G., and Martin-Serrano, J. (2007). Parallels between cytokinesis and retroviral budding: a role for the ESCRT machinery. Science *316*, 1908–1912.

Carpy, A., Krug, K., Graf, S., Koch, A., Popic, S., Hauf, S., and Macek, B. (2014). Absolute proteome and phosphoproteome dynamics during the cell cycle of Schizosaccharomyces pombe (Fission Yeast). Mol. Cell. Proteomics *13*, 1925–1936.

Carpy, A., Patel, A., Tay, Y.D., Hagan, I.M., and Macek, B. (2015). Nic1 inactivation enables stable isotope labeling with 13C615N4-arginine in Schizosaccharomyces pombe. Mol. Cell. Proteomics *14*, 243–250.

Cheng, Z., Otto, G.M., Powers, E.N., Keskin, A., Mertins, P., Carr, S.A., Jovanovic, M., and Brar, G.A. (2018). Pervasive, coordinated protein-level changes driven by transcript isoform switching during meiosis. Cell *172*, 910–923.e6.

Chikashige, Y., Ding, D.Q., Funabiki, H., Haraguchi, T., Mashiko, S., Yanagida, M., and Hiraoka, Y. (1994). Telomere-led premeiotic chromosome movement in fission yeast. Science *264*, 270–273.

Chikashige, Y., Kurokawa, R., Haraguchi, T., and Hiraoka, Y. (2004). Meiosis induced by inactivation of Pat1 kinase proceeds with aberrant nuclear positioning of centromeres in the fission yeast Schizosaccharomyces pombe. Genes Cells *9*, 671–684.

Chikashige, Y., Yamane, M., Okamasa, K., Osakada, H., Tsutsumi, C., Nagahama, Y., Fukuta, N., Haraguchi, T., and Hiraoka, Y. (2017). Fission yeast APC/C activators Slp1 and Fzr1 sequentially trigger two consecutive nuclear divisions during meiosis. FEBS Lett. *591*, 1029–1040.

Cox, J., and Mann, M. (2008). MaxQuant enables high peptide identification rates, individualized p.p.b.-range mass accuracies and proteome-wide protein quantification. Nat. Biotechnol. *26*, 1367–1372.

de Medina-Redondo, M., Arnáiz-Pita, Y., Fontaine, T., Del Rey, F., Latgé, J.P., and Vázquez de Aldana, C.R. (2008). The beta-1,3-glucanosyltransferase gas4p is essential for ascospore wall maturation and spore viability in Schizosaccharomyces pombe. Mol. Microbiol. *68*, 1283–1299.

Deutschbauer, A.M., Williams, R.M., Chu, A.M., and Davis, R.W. (2002). Parallel phenotypic analysis of sporulation and postgermination growth in Saccharomyces cerevisiae. Proc. Natl. Acad. Sci. USA *99*, 15530–15535.

Doyle, A., Martín-García, R., Coulton, A.T., Bagley, S., and Mulvihill, D.P. (2009). Fission yeast Myo51 is a meiotic spindle pole body component with discrete roles during cell fusion and spore formation. J. Cell Sci. *122*, 4330–4340.

Duncan, C.D., and Mata, J. (2014). The translational landscape of fission-yeast meiosis and sporulation. Nat. Struct. Mol. Biol. *21*, 641–647.

Fantes, P.A., and Hoffman, C.S. (2016). A brief history of Schizosaccharomyces pombe research: a perspective over the past 70 years. Genetics *203*, 621–629.

Frost, A., Elgort, M.G., Brandman, O., Ives, C., Collins, S.R., Miller-Vedam, L., Weibezahn, J., Hein, M.Y., Poser, I., Mann, M., et al. (2012). Functional repurposing revealed by comparing S. pombe and S. cerevisiae genetic interactions. Cell *149*, 1339–1352.

Fukunishi, K., Miyakubi, K., Hatanaka, M., Otsuru, N., Hirata, A., Shimoda, C., and Nakamura, T. (2014). The fission yeast spore is coated by a proteinaceous surface layer comprising mainly Isp3. Mol. Biol. Cell *25*, 1549–1559.

Funaya, C., Samarasinghe, S., Pruggnaller, S., Ohta, M., Connolly, Y., Müller, J., Murakami, H., Grallert, A., Yamamoto, M., Smith, D., et al. (2012). Transient structure associated with the spindle pole body directs meiotic microtubule reorganization in S. pombe. Curr. Biol. *22*, 562–574.

Geiger, T., Cox, J., Ostasiewicz, P., Wisniewski, J.R., and Mann, M. (2010). Super-SILAC mix for quantitative proteomics of human tumor tissue. Nat. Methods *7*, 383–385.

Gu, M., LaJoie, D., Chen, O.S., von Appen, A., Ladinsky, M.S., Redd, M.J., Nikolova, L., Bjorkman, P.J., Sundquist, W.I., Ullman, K.S., and Frost, A. (2017). LEM2 recruits CHMP7 for ESCRT-mediated nuclear envelope closure in fission yeast and human cells. Proc. Natl. Acad. Sci. U S A *114*, E2166–E2175.

Gunaratne, J., Schmidt, A., Quandt, A., Neo, S.P., Saraç, O.S., Gracia, T., Loguercio, S., Ahrné, E., Xia, R.L., Tan, K.H., et al. (2013). Extensive mass spectrometry-based analysis of the fission yeast proteome: the Schizosaccharomyces pombe PeptideAtlas. Mol. Cell. Proteomics *12*, 1741–1751.

Hagan, I.M., Carr, A.M., Grallert, A., and Nurse, P., eds. (2016). Fission Yeast: A Laboratory Manual (Cold Spring Harbor Laboratory Press).

Harigaya, Y., Tanaka, H., Yamanaka, S., Tanaka, K., Watanabe, Y., Tsutsumi, C., Chikashige, Y., Hiraoka, Y., Yamashita, A., and Yamamoto, M. (2006). Selective elimination of messenger RNA prevents an incidence of untimely meiosis. Nature *442*, 45–50.

Hurley, J.H., and Emr, S.D. (2006). The ESCRT complexes: structure and mechanism of a membrane-trafficking network. Annu. Rev. Biophys. Biomol. Struct. *35*, 277–298.

Iino, Y., and Yamamoto, M. (1985). Negative control for the initiation of meiosis in Schizosaccharomyces pombe. Proc. Natl. Acad. Sci. U S A *82*, 2447–2451.

Ikemoto, S., Nakamura, T., Kubo, M., and Shimoda, C. (2000). S. pombe sporulation-specific coiled-coil protein Spo15p is localized to the spindle pole body and essential for its modification. J. Cell Sci. *113*, 545–554.

Itadani, A., Nakamura, T., and Shimoda, C. (2006). Localization of type I myosin and F-actin to the leading edge region of the forespore membrane in Schizosaccharomyces pombe. Cell Struct. Funct. *31*, 181–195.

Izawa, D., Goto, M., Yamashita, A., Yamano, H., and Yamamoto, M. (2005). Fission yeast Mes1p ensures the onset of meiosis II by blocking degradation of cyclin Cdc13p. Nature *434*, 529–533.

Jin, Y., Mancuso, J.J., Uzawa, S., Cronembold, D., and Cande, W.Z. (2005). The fission yeast homolog of the human transcription factor EAP30 blocks meiotic spindle pole body amplification. Dev. Cell *9*, 63–73.

Kasama, T., Shigehisa, A., Hirata, A., Saito, T.T., Tougan, T., Okuzaki, D., and Nojima, H. (2006). Spo5/Mug12, a putative meiosis-specific RNA-binding protein, is essential for meiotic progression and forms Mei2 dot-like nuclear foci. Eukaryot. Cell *5*, 1301–1313.

Kashiwazaki, J., Yamasaki, Y., Itadani, A., Teraguchi, E., Maeda, Y., Shimoda, C., and Nakamura, T. (2011). Endocytosis is essential for dynamic translocation of a syntaxin 1 orthologue during fission yeast meiosis. Mol. Biol. Cell *22*, 3658–3670.

Kimata, Y., Trickey, M., Izawa, D., Gannon, J., Yamamoto, M., and Yamano, H. (2008). A mutual inhibition between APC/C and its substrate Mes1 required for meiotic progression in fission yeast. Dev. Cell *14*, 446–454.

Kitajima, T.S., Kawashima, S.A., and Watanabe, Y. (2004). The conserved kinetochore protein shugoshin protects centromeric cohesion during meiosis. Nature *427*, 510–517.

Kitajima, T.S., Sakuno, T., Ishiguro, K., Iemura, S., Natsume, T., Kawashima, S.A., and Watanabe, Y. (2006). Shugoshin collaborates with protein phosphatase 2A to protect cohesin. Nature *441*, 46–52.

Kitamura, K., Katayama, S., Dhut, S., Sato, M., Watanabe, Y., Yamamoto, M., and Toda, T. (2001). Phosphorylation of Mei2 and Ste11 by Pat1 kinase inhibits sexual differentiation via ubiquitin proteolysis and 14-3-3 protein in fission yeast. Dev. Cell *1*, 389–399.

Klaips, C.L., Jayaraj, G.G., and Hartl, F.U. (2018). Pathways of cellular proteostasis in aging and disease. J. Cell Biol. *217*, 51–63.

Kluyver, T., Ragan-Kelley, B., Perez, F., Granger, B., Bussonnier, M., Frederic, J., Kelley, K., Hamrick, J., Grout, J., Corlay, S., et al. (2016). Jupyter Notebooks—A Publishing Format for Reproducible Computational Workflows (IOS Press).

Krapp, A., and Simanis, V. (2014). Dma1-dependent degradation of SIN proteins during meiosis in Schizosaccharomyces pombe. J. Cell Sci. *127*, 3149–3161.

Krapp, A., Collin, P., Cokoja, A., Dischinger, S., Cano, E., and Simanis, V. (2006). The Schizosaccharomyces pombe septation initiation network (SIN) is required for spore formation in meiosis. J. Cell Sci. *119*, 2882–2891.

Kulak, N.A., Pichler, G., Paron, I., Nagaraj, N., and Mann, M. (2014). Minimal, encapsulated proteomic-sample processing applied to copy-number estimation in eukaryotic cells. Nat. Methods *11*, 319–324.

Liu, X.M., Sun, L.L., Hu, W., Ding, Y.H., Dong, M.Q., and Du, L.L. (2015). ESCRTs cooperate with a selective autophagy receptor to mediate vacuolar targeting of soluble cargos. Mol. Cell *59*, 1035–1042.

Liu, Y., Beyer, A., and Aebersold, R. (2016). On the dependency of cellular protein levels on mRNA abundance. Cell *165*, 535–550.

Maeda, Y., Kashiwazaki, J., Shimoda, C., and Nakamura, T. (2009). The Schizosaccharomyces pombe syntaxin 1 homolog, Psy1, is essential in the development of the forespore membrane. Biosci. Biotechnol. Biochem. *73*, 339–345.

Martín-Castellanos, C., Blanco, M., Rozalén, A.E., Pérez-Hidalgo, L., García, A.I., Conde, F., Mata, J., Ellermeier, C., Davis, L., San-Segundo, P., et al. (2005). A large-scale screen in S. pombe identifies seven novel genes required for critical meiotic events. Curr. Biol. *15*, 2056–2062.

Mata, J., and Bähler, J. (2006). Global roles of Ste11p, cell type, and pheromone in the control of gene expression during early sexual differentiation in fission yeast. Proc. Natl. Acad. Sci. U S A *103*, 15517–15522.

Mata, J., Lyne, R., Burns, G., and Bähler, J. (2002). The transcriptional program of meiosis and sporulation in fission yeast. Nat. Genet. *32*, 143–147.

Mata, J., Wilbrey, A., and Bähler, J. (2007). Transcriptional regulatory network for sexual differentiation in fission yeast. Genome Biol. *8*, R217.

Matsuhara, H., and Yamamoto, A. (2016). Autophagy is required for efficient meiosis progression and proper meiotic chromosome segregation in fission yeast. Genes Cells *21*, 65–87.

McLeod, M., and Beach, D. (1988). A specific inhibitor of the ran1+ protein kinase regulates entry into meiosis in Schizosaccharomyces pombe. Nature *332*, 509–514.

McLeod, M., Stein, M., and Beach, D. (1987). The product of the mei3+ gene, expressed under control of the mating-type locus, induces meiosis and sporulation in fission yeast. EMBO J. *6*, 729–736.

Moreno, S., Klar, A., and Nurse, P. (1991). Molecular genetic analysis of fission yeast Schizosaccharomyces pombe. Methods Enzymol. *194*, 795–823.

Morita, E., Sandrin, V., Chung, H.Y., Morham, S.G., Gygi, S.P., Rodesch, C.K., and Sundquist, W.I. (2007). Human ESCRT and ALIX proteins interact with proteins of the midbody and function in cytokinesis. EMBO J. *26*, 4215–4227.

Morita, E., Colf, L.A., Karren, M.A., Sandrin, V., Rodesch, C.K., and Sundquist, W.I. (2010). Human ESCRT-III and VPS4 proteins are required for centrosome and spindle maintenance. Proc. Natl. Acad. Sci. U S A *107*, 12889–12894.

Mukaiyama, H., Kajiwara, S., Hosomi, A., Giga-Hama, Y., Tanaka, N., Nakamura, T., and Takegawa, K. (2009). Autophagy-deficient Schizosaccharomyces pombe mutants undergo partial sporulation during nitrogen starvation. Microbiology *155*, 3816–3826.

Mukaiyama, H., Nakase, M., Nakamura, T., Kakinuma, Y., and Takegawa, K. (2010). Autophagy in the fission yeast Schizosaccharomyces pombe. FEBS Lett. *584*, 1327–1334.

Murphy, J.P., Stepanova, E., Everley, R.A., Paulo, J.A., and Gygi, S.P. (2015). Comprehensive Temporal Protein Dynamics during the Diauxic Shift in Saccharomyces cerevisiae. Mol. Cell. Proteomics *14*, 2454–2465.

Nakamura, T., Nakamura-Kubo, M., Hirata, A., and Shimoda, C. (2001). The Schizosaccharomyces pombe spo3+ gene is required for assembly of the forespore membrane and genetically interacts with psy1(+)-encoding syntaxin-like protein. Mol. Biol. Cell *12*, 3955–3972.

Nakamura, T., Nakamura-Kubo, M., Nakamura, T., and Shimoda, C. (2002). Novel fission yeast Cdc7-Dbf4-like kinase complex required for the initiation and progression of meiotic second division. Mol. Cell. Biol. *22*, 309–320.

Nakamura, T., Asakawa, H., Nakase, Y., Kashiwazaki, J., Hiraoka, Y., and Shimoda, C. (2008). Live observation of forespore membrane formation in fission yeast. Mol. Biol. Cell *19*, 3544–3553.

Nakase, Y., Nakamura-Kubo, M., Ye, Y., Hirata, A., Shimoda, C., and Nakamura, T. (2008). Meiotic spindle pole bodies acquire the ability to assemble the spore plasma membrane by sequential recruitment of sporulation-specific components in fission yeast. Mol. Biol. Cell *19*, 2476–2487.

Nakashima, A., Hasegawa, T., Mori, S., Ueno, M., Tanaka, S., Ushimaru, T., Sato, S., and Uritani, M. (2006). A starvation-specific serine protease gene, isp6+, is involved in both autophagy and sexual development in Schizosaccharomyces pombe. Curr. Genet. *49*, 403–413.

Niwa, O., and Yanagida, M. (1985). Triploid meiosis and aneuploidy in Schizosaccharomyces pombe: an unstable aneuploid disomic for chromosome III. Curr. Genet. *9*, 463–470.

Nurse, P. (1985). Mutants of the fission yeast Schizosaccharomyces pombe which alter the shift between cell proliferation and sporulation. Molecular and General Genetics MGG *198*, 497–502.

Ohtaka, A., Okuzaki, D., and Nojima, H. (2008). Mug27 is a meiosis-specific protein kinase that functions in fission yeast meiosis II and sporulation. J. Cell Sci. *121*, 1547–1558.

Okuzaki, D., Satake, W., Hirata, A., and Nojima, H. (2003). Fission yeast meu14+ is required for proper nuclear division and accurate forespore membrane formation during meiosis II. J. Cell Sci. *116*, 2721–2735.

Ong, S.E., Blagoev, B., Kratchmarova, I., Kristensen, D.B., Steen, H., Pandey, A., and Mann, M. (2002). Stable isotope labeling by amino acids in cell culture, SILAC, as a simple and accurate approach to expression proteomics. Mol. Cell. Proteomics *1*, 376–386.

Onishi, M., Iida, M., Koga, T., Yamada, S., Hirata, A., Iwaki, T., Takegawa, K., Fukui, Y., and Tachikawa, H. (2007). Schizosaccharomyces pombe Sst4p, a conserved Vps27/Hrs homolog, functions downstream of phosphatidylinositol 3-kinase Pik3p to mediate proper spore formation. Eukaryot. Cell *6*, 2343–2353.

Onishi, M., Koga, T., Hirata, A., Nakamura, T., Asakawa, H., Shimoda, C., Bähler, J., Wu, J.Q., Takegawa, K., Tachikawa, H., et al. (2010). Role of septins in the orientation of forespore membrane extension during sporulation in fission yeast. Mol. Cell. Biol. *30*, 2057–2074.

Pedregosa, F., Varoquaux, G., Gramfort, A., Michel, V., Thirion, B., Grisel, O., Blondel, M., Prettenhofer, P., Weiss, R., Dubourg, V., et al. (2011). scikit-learn: machine learning in Python. J. Mach. Learn. Res. *12*, 2825–2830.

Pérez-Hidalgo, L., Rozalén, A.E., Martín-Castellanos, C., and Moreno, S. (2008). Slk1 is a meiosis-specific Sid2-related kinase that coordinates meiotic nuclear division with growth of the forespore membrane. J. Cell Sci. *121*, 1383–1392.

Petersen, J., Nielsen, O., Egel, R., and Hagan, I.M. (1998). F-actin distribution and function during sexual differentiation in Schizosaccharomyces pombe. J. Cell Sci. *111*, 867–876.

Rabitsch, K.P., Gregan, J., Schleiffer, A., Javerzat, J.P., Eisenhaber, F., and Nasmyth, K. (2004). Two fission yeast homologs of Drosophila Mei-S332 are required for chromosome segregation during meiosis I and II. Curr. Biol. *14*, 287–301.

Rappsilber, J., Mann, M., and Ishihama, Y. (2007). Protocol for micro-purification, enrichment, pre-fractionation and storage of peptides for proteomics using StageTips. Nat. Protoc. *2*, 1896–1906.

Riedel, C.G., Katis, V.L., Katou, Y., Mori, S., Itoh, T., Helmhart, W., Gálová, M., Petronczki, M., Gregan, J., Cetin, B., et al. (2006). Protein phosphatase 2A

protects centromeric sister chromatid cohesion during meiosis I. Nature *441*, 53–61.

Robinow, C.F. (1977). The number of chromosomes in Schizosaccharomyces pombe: light microscopy of stained preparations. Genetics *87*, 491–497.

Saito, T.T., Okuzaki, D., and Nojima, H. (2006). Mcp5, a meiotic cell cortex protein, is required for nuclear movement mediated by dynein and microtubules in fission yeast. J. Cell Biol. *173*, 27–33.

Sculley, D. (2010). Web-scale k-means clustering. In Proceedings of the 19th International Conference on World Wide Web (ACM), pp. 1177–1178.

Shichino, Y., Yamashita, A., and Yamamoto, M. (2014). Meiotic long non-coding meiRNA accumulates as a dot at its genetic locus facilitated by Mmi1 and plays as a decoy to lure Mmi1. Open Biol. *4*, 140022.

Shichino, Y., Otsubo, Y., Kimori, Y., Yamamoto, M., and Yamashita, A. (2018). YTH-RNA-binding protein prevents deleterious expression of meiotic proteins by tethering their mRNAs to nuclear foci. eLife *7*, e32155.

Shimoda, C. (2004). Forespore membrane assembly in yeast: coordinating SPBs and membrane trafficking. J. Cell Sci. *117*, 389–396.

Szklarczyk, D., Franceschini, A., Wyder, S., Forslund, K., Heller, D., Huerta-Cepas, J., Simonovic, M., Roth, A., Santos, A., Tsafou, K.P., et al. (2015). STRING v10: protein-protein interaction networks, integrated over the tree of life. Nucleic Acids Res. *43*, D447–D452.

Tai, Y. (2007). timecourse: statistical analysis for developmental microarray time course data. (http://www.bioconductor.org).

Tanaka, K., Kohda, T., Yamashita, A., Nonaka, N., and Yamamoto, M. (2005). Hrs1p/Mcp6p on the meiotic SPB organizes astral microtubule arrays for oscillatory nuclear movement. Curr. Biol. *15*, 1479–1486.

R Core Team (2016). R: A Language and Environment for Statistical Computing (Vienna, Austria: R Foundation for Statistical Computing).

Tougan, T., Chiba, Y., Kakihara, Y., Hirata, A., and Nojima, H. (2002). Meu10 is required for spore wall maturation in Schizosaccharomyces pombe. Genes Cells *7*, 217–231.

Wen, F.P., Guo, Y.S., Hu, Y., Liu, W.X., Wang, Q., Wang, Y.T., Yu, H.Y., Tang, C.M., Yang, J., Zhou, T., et al. (2016). Distinct temporal requirements for autophagy and the proteasome in yeast meiosis. Autophagy *12*, 671–688.

Wilkinson, C.R., Wallace, M., Morphew, M., Perry, P., Allshire, R., Javerzat, J.P., McIntosh, J.R., and Gordon, C. (1998). Localization of the 26S proteasome during mitosis and meiosis in fission yeast. EMBO J. *17*, 6465–6476.

Wiśniewski, J.R., Zougman, A., and Mann, M. (2009). Combination of FASP and StageTip-based fractionation allows in-depth analysis of the hippocampal membrane proteome. J. Proteome Res. *8*, 5674–5678.

Woods, A., Sherwin, T., Sasse, R., MacRae, T.H., Baines, A.J., and Gull, K. (1989). Definition of individual components within the cytoskeleton of Trypanosoma brucei by a library of monoclonal antibodies. J. Cell Sci. *93*, 491–500.

Xu, G., and West, T.P. (1992). Protein synthesis during germination of heterothallic yeast ascospores. Experientia *48*, 786–788.

Yamanaka, S., Yamashita, A., Harigaya, Y., Iwata, R., and Yamamoto, M. (2010). Importance of polyadenylation in the selective elimination of meiotic mRNAs in growing S. pombe cells. EMBO J. *29*, 2173–2181.

Yamashita, A., Shichino, Y., Tanaka, H., Hiriart, E., Touat-Todeschini, L., Vavasseur, A., Ding, D.Q., Hiraoka, Y., Verdel, A., and Yamamoto, M. (2012). Hexanucleotide motifs mediate recruitment of the RNA elimination machinery to silent meiotic genes. Open Biol. *2*, 120014.

Yamashita, A., Sakuno, T., Watanabe, Y., and Yamamoto, M. (2017). Analysis of Schizosaccharomyces pombe meiosis. Cold Spring Harb. Protoc. *2017*, pdb.top079855.

Yan, H., and Balasubramanian, M.K. (2012). Meiotic actin rings are essential for proper sporulation in fission yeast. J. Cell Sci. *125*, 1429–1439.

Yan, H., Ge, W., Chew, T.G., Chow, J.Y., McCollum, D., Neiman, A.M., and Balasubramanian, M.K. (2008). The meiosis-specific Sid2p-related protein Slk1p regulates forespore membrane assembly in fission yeast. Mol. Biol. Cell *19*, 3676–3690.

STAR★METHODS

KEY RESOURCES TABLE

REAGENT or RESOURCE	SOURCE	IDENTIFIER
Yeast strains		
Strains used	See Table S8	N/A
Antibodies		
cdc13	Santa Cruz	sc-53215; RRID:AB_629250
TAT1	Keith Gull (Oxford) (Woods et al., 1989)	N/A
actin	Life Technologies	MA1-744; RRID:AB_2223496
GFP	In-house (Krapp and Simanis, 2014)	N/A
9E10 (myc)	Iggo lab (ISREC)	N/A
12CA5 (HA)	Roche	11 583 816 001; RRID:AB_514505
HRP-coupled secondary anti-mouse	Promega	W4021
HRP-coupled secondary anti-rabbit	Promega	W4011
Commercial assays and reagents		
l-arginine:HCl (U-13C6, 99%; U-15N4, 99%)	Cambridge Isotopes	CNLM-539-H-0.1
l-lysine:2HCl (U-13C6, 99%; U-15N2, 99%)	Cambridge Isotopes	CNLM-291-H-0.1
nitrocellulose membranes, Protran™ BA 85	Whatman	10 401 196
Protein Assay	BioRad	500-0006
ECL Western Blotting Detection Reagent	GE Healthcare	RPN 2106
Lysing enzyme	Sigma	L-1412
Lysing Matrix C beads	MP Biomedicals	116912100
4′,6-Diamidino-2-phenylindole dihydrochloride	Sigma	D9542
Trypsin Gold	Promega	V5280
TCEP	Sigma	C4706
CAA	Sigma	C0267
Lys-C	Wako	129-02541
TFA	Thermo Scientific	85183
FA	Merck	1.00264.0100
ACN	Biosolve	0001204102BS
Ammonium Acetate	Fluka	09690
Ammonia Solution	Sigma	30501
Trizma hydrochloride solution	Sigma	T2694
SCX disks	3M	2251
C18 disks	3M	2215
HiPPR Detergent Removal Spin Columns	Thermo Scientific	88306
Microcon-30 Centrifugal filters	Millipore	MRCF0R030
Deposited Data		
Raw and analyzed data	This paper	PXD010438 http://proteomecentral.proteomexchange.org/cgi/GetDataset?ID=PXD010438
Software and Algorithms		
ImageJ	N/A	N/A
Python programming language	Python Software Foundation	https://www.python.org/
MaxQuant 1.5.1.2	N/A	http://www.coxdocs.org/doku.php?id=maxquant:start
R software	N/A	https://www.r-project.org/
String v10	N/A	http://string-db.org/

CONTACT FOR REAGENT AND RESOURCE SHARING

Further information and requests for reagents may be directed to, and will be fulfilled by, the Lead Contact, Viesturs Simanis (viesturs.simanis@epfl.ch).

EXPERIMENTAL MODEL AND SUBJECT DETAILS

Yeast methods

Standard techniques were used for fission yeast growth and analysis (Hagan et al., 2016; Moreno et al., 1991). Strains used in this study are listed in the table below. Some strains were obtained from the Japanese National BioResource Project, or from the Bioneer *S. pombe* viable null mutant strain collection (V5). Lab stock strains were obtained by mating the required parental strains on minimal medium (EMM2) without NH_4Cl (EMM2-N) followed by tetrad dissection on a Singer® MSM micromanipulator. The desired progeny were identified after replica plating on appropriate media. Diploid cells were obtained after mating of parental strains by complementation of two adenine alleles (*ade6-M210* and *ade6-M216*) and selection on minimal medium lacking adenine, as described (Hagan et al., 2016).

List of main yeast strains used

Please see Table S8.

Meiotic synchronization

Diploid cells were synchronized in meiosis using the temperature sensitive *pat1-114* allele. Therefore, diploid *pat1-114/pat1-114 leu1-32/leu1-32 ade6-M210/ade6-M216 h+/h+* cells were grown at 25°C in minimal medium (EMM) before being starved for 16 hr at 25°C in minimal medium without NH_4Cl (EMM-N). Meiosis was then induced by shifting the culture to 32°C and adding NH_4Cl to 0.01% (w/v). Samples were taken hourly up to 10 hours for protein extraction and DAPI staining (Hagan et al., 2016), which allowed us to monitor meiotic progression by determining the percentage of cells with one, two or four nuclei. As has been noted by others (Chikashige et al., 2004; Yamashita et al., 2017) induction of meiosis using this method requires both starvation and a heat-shock to inactivate Pat1p. We cannot exclude that some of the changes we observe here are a consequence of these manipulations, rather than meiotic progression.

SILAC labeling

Incorporation of heavy amino acids was done according to (Carpy et al., 2015). Diploid pat1-114/pat1-114 car2::Nat^R/car2::Nat^R nic1::KanMX4/nic1::KanMX4 mat2-P102 leu1-32/leu1-32 ura4-D18/ura4-D18 arg3-D4/arg3-D4 lys1-131/lys1-131 ade6-M210/ade6-M216 cells were grown for 17 generations in exponential growth in EMMG (Hagan et al., 2016), supplemented with 100mg/l leucine, 100mg/l uracil, 500mg/l proline, 0.65 g/l NH_4Cl, 75mg/l heavy isotopic versions of lysine and 12.5mg/l heavy isotopic versions of arginine (l-lysine:2HCl (U-13C6, 99%; U-15N2, 99%, Cambridge Isotopes; CNLM-291-H-0.1), and l-arginine:HCl (U-13C6, 99%; U-15N4, 99%, Cambridge Isotopes; CNLM-539-H-0.1)). Cells were then washed and resuspended in EMM-N supplemented with 20mg/l leucine, 20mg/l uracil, 20mg/l proline, 20mg/l heavy isotopic versions of lysine and 3mg/l heavy isotopic versions of arginine for starvation during 16 hr at 25°C. Meiosis was induced by shifting the culture to 32°C and addition of amino acids to 100mg/l leucine, 100mg/l uracil, 500mg/l proline, 0.65 g/l NH_4Cl, 75mg/l heavy isotopic versions of lysine and 12.5mg/l heavy isotopic versions of arginine. Aliquots were removed at time 0hrs, 3hrs, 5hrs and 8hrs for protein extraction and fixed for microscopy as above. Time points 0 and 3 hr contained mostly mononucleated cells (98.4% and 99.6%, respectively) at 5hrs, the number of binucleated cells increased (30.1%) while few tetranucleated cells were present (0.5%). At 8hrs most asci contained four nuclei (84.3%). Analysis showed approximately 99% incorporation of $^{13}C_6$-$^{15}N_2$-lysine and $^{13}C_6$-$^{15}N_4$-arginine into the proteome. For the heavy Super-SILAC mix, protein extracts of all four time points were mixed in a 1:1:1:1 ratio with respect to protein concentration. The Super-SILAC "heavy" reference sample was then mixed with each "light" sample at a 1:1 ratio with respect to protein concentration.

METHOD DETAILS

Sample processing for mass spectrometry

Samples were trypsin digested using the Filter-Aided Sample preparation (FASP) protocol (Wiśniewski et al., 2009) with minor modifications. Lysates corresponding to 30 μg of proteins were resuspended in 200 μl of 8M urea/100 mM Tris-HCl and deposited on top of Microcon-30K devices (Millipore). Samples were centrifuged at 9391 g at 20°C for 30 min. All subsequent centrifugation steps were performed using the same conditions. An additional 200 μl of 8M urea/100 mM Tris was added and devices were centrifuged again. Reduction was performed by adding 100 μl of 10mM TCEP in 8M urea/100 mM Tris-HCl on top of filters followed by 60 min incubation time at 37°C with gentle shaking and light protected.

Alkylation solution was removed by centrifugation and filters were washed with 200 μl of 8M urea/100 mM Tris-HCl After removal of washing solution by centrifugation, alkylation was performed in 100 μl of 40mM CAA in 8M urea/100 mM Tris-HCl at 37°C for 45 min.,

with gentle shaking and protected from light. The alkylation solution was removed by centrifugation and another washing/centrifugation step with 200 μl of 8M urea/100 mM Tris-HCl was performed. This last urea buffer washing step was repeated twice followed by three additional washing steps with 100 μl of 5mM Tris-HCl.

Proteolytic digestion was performed overnight at 37° after adding on top of filters 100μl of a combined solution of Endoproteinase Lys-C and Trypsin Gold in an enzyme/protein ratio of 1:50 (w/w) supplemented with 10mM CaCl2. Resulting peptides were recovered by centrifugation. The devices were then rinsed with 50 μl of 5mM Tris-HCl and centrifuged. This step was repeated three times. Eluted samples were concentrated in a speed-vac during 40 min and incubated 1 hour in Detergent Removal Spin Columns (Thermo Scientific) to remove eventual residual SDS. Samples were then centrifuged and acidified to pH < 3 using 10 μl of 10% TFA.

Samples were then desalted on C18 Stage Tips (Rappsilber et al., 2007). C18 Stage Tips were washed twice using a benchtop centrifuge (500xg) with 80% acetonitrile and conditioned three times with 0.1% TFA. Acidified samples were loaded and then washed twice with 0.1% TFA. Elution was performed first with 80% acetonitrile containing 0.1% TFA and then with 80% acetonitrile containing 10% TFE and 0.1% TFA. Eluted samples were dried in a speed-vac during 40 min. Samples were fractionated using Strong Cation eXchange (SCX) as previously described (Kulak et al., 2014). Briefly, Stage Tips were prepared by placing six layers of a 3M Empore Cation Exchange disk (3M) into a P200 pipette tip. All fractionation steps were performed using a benchtop centrifuge (500 x g). Stage Tips were conditioned with 100 μl ACN followed by a wash of 100 μl of 1% TFA. Samples were reconstituted in 100 μl of 1% TFA and loaded onto the Tips. Peptides were washed twice using 100 μl of 0.2% TFA and sequentially eluted using volatile elution buffers. Eluted fractions were dried by vacuum centrifugation prior to LC-MS/MS analysis.

Liquid chromatography and MS

Each SCX fraction was resuspended in 2% acetonitrile (ACN) 0.1% Formic Acid (FA) and separated by Reverse-Phase chromatography on a Dionex Ultimate 3000 RSLC nanoUPLC system in-line connected with an Orbitrap Q Exactive Mass-Spectrometer (Thermo Fischer Scientific). Samples were first trapped on a capillary Dionex precolumn (Acclaim PepMap 100, 75μmID x 2cm, C18 3μm 100Ä) and then separated on a Dionex (Acclaim Pepmap RSLC 75μmID x 50cm, C18 2μm 100Ä) at 250nl/min applying a non-linear 240min gradient ranging from 99% solvent A (2% ACN and 0.1% FA) to 90% solvent B (90% ACN and 0.1%FA). Acquisitions were performed using Data-Dependent acquisition mode. First MS scans were acquired with a resolution of 70'000 (at 200 m/z) and the 10 most intense parent ions were selected and fragmented by High energy Collision Dissociation (HCD) with a Normalized Collision Energy (NCE) of 27% using an isolation window of 2.0 m/z. Fragmented ions were then excluded for the following 45 s.

Protein extraction

Protein extraction was performed as described (Bicho et al., 2010). Cells were harvested for 2 minutes at 3000 rpm at room temperature (approx. 25°C), washed once in TBS (50 mM Tris-HCl pH 7.5, 150 mM NaCl). The cell pellet was then resuspended in 150 μL TBS and heated to 5 minutes at 95°C to inactivate proteases. Cells were then disrupted in a MagNA Lyser (Roche) using Lysing Matrix C beads (MP Biomedicals) at 4°C during 2 cycles of 45 s at setting 6.5. Disrupted cells were then recovered and extracted by addition of an equal volume of sample buffer (0.125 M Tris-HCl pH 6.8, 4% (w/v) SDS, 20% (v/v) glycerol) and heated for 5 minutes at 95°C. The extract was then finally centrifuged 10 minutes at 12500 rpm at room temperature to remove cell debris. The protein concentration of the supernatants was determined using the Bradford protein assay (BioRad) on samples diluted 5 times in 1xPBS. Samples were diluted as required in 1X sample buffer. Prior to gel electrophoresis, extracts were supplemented with bromophenol blue and β-mercaptoethanol was added to 5% (v/v).

Data validation by western blotting

For data validation, diploid cells carrying the *pat1-114* allele and the indicated tagged allele were induced to undergo meiosis, protein extracts were prepared hourly for 9 hours and cell cycle progression analyzed by DAPI/Calcofluor staining as described above. Proteins (125ng/lane) were separated by SDS-PAGE (ThermoFischer) and transferred to nitrocellulose membranes (Protran™ BA85, Whatman). The membrane was stained 2 minutes with Ponceau S (0.1% w/v Ponceau S in 5% (v/v) acetic acid/water) and then blocked in 5% (w/v) powdered milk in PBST (0.1% Tween-20 in 1xPBS) for 1 hour at room temperature. The primary antibody was added to the membrane and incubated overnight at 4°C. The primary antibodies used are listed in the key reagents table. Membranes were washed 3 times for 15 minutes in PBST before addition of the HRP-coupled secondary antibodies (Promega) for 1 hr at room temperature. Finally, the membranes were washed 3 times for 15 minutes in PBST, developed in Western ECL Substrate (GE Healthcare); Images were acquired using a Fusion FX (Vilber) system.

DAPI staining

Meiotic progression was followed by nuclear staining with DAPI. Cells were harvested 2 minutes at 3000 rpm, washed in water and resuspended in 70% (v/v) ethanol. Fixed cells were then washed in 1xPBS and stained in 1xPBS containing 20 μg/ml DAPI (4′,6-Diamidino-2-phenylindole dihydrochloride, Sigma). Images were captured on a Zeiss Axiophot microscope using a Nikon D5600 camera and processed using Photoshop CS6. At least 200 cells were counted for each sample.

Spore formation and germination efficiency assays

Spore formation efficiency was determined as follow: cells of opposite mating type containing the indicated deletions were mated on EMM-N for 4 days. Asci were then fixed with 70% (v/v) ethanol and the phenotypes observed by DAPI staining. Phenotypes were scored as follow: asci containing 4 nuclei and 4 spores (“wt”), asci containing more or less than 4 nuclei (dark/light orange and yellow boxes; failure in nuclear cycles), asci containing 4 nuclei but less than 4 spores or no spores (green boxes; spore formation defects), and others. Images were captured on a Zeiss Axiophot microscope using a Nikon D5600 camera and processed using Photoshop CS6. Phenotypes are expressed in percent and plotted on a bar plot. For each strain, three independent experiments were performed and standard deviations calculated.

For the germination efficiency assay, cells of opposite mating type containing the indicated deletions were mated on EMM-N during 4 days. Spores were prepared as follow: asci were washed in water and resuspended lysing enzymes (Sigma) O/N at 25°C. Cells were then incubated for 30 minutes in 20% (v/v) ethanol to kill haploid and diploid cells, washed and resuspended in water. Spores were then individually placed on a YE5S plate using a Singer MSM micromanipulator. Colonies were allowed to grow at 29°C. The percentage of colony-forming spores was determined and plotted on a bar plot. For each strain, three independent experiments were done and standard deviations calculated. The numbers of asci and spores scored in each experiment are listed in Table S9.

QUANTIFICATION AND STATISTICAL ANALYSIS

Computational Proteomics

SILAC data were analyzed with MaxQuant (Cox and Mann, 2008) version 1.5.1.2 against a *Schizosaccharomyces pombe* database containing 5146 sequences (Pombase release 2015-09-29). Enzyme specificity was set to Trypsin and a minimum of seven amino acids was required for peptide identification. Up to two missed cleavages were allowed. A 1% FDR cut-off was fixed at peptide and protein identification levels. Carbamidomethylation (C) was set as a fixed modification, whereas oxidation (M), acetylation (protein N-term), Gln to pyro-Glu, Glu to pyro-Glu and Phospho (STY) were considered as variable modifications. SILAC quantifications were performed by MaxQuant using the standard settings and with the re-quantification mode enabled.

Bioinformatic, statistical analysis and clustering

Data analyses were performed with home-made programs developed in R statistical computing environment (R Core Team, 2016). Triplicate datasets were first inverted to analyze the L/H normalized ratios and $\log_2$ transformed. Only quantified proteins missing up to one time course point per biological sample were considered. The quantitative values for the missing points were calculated as the average of its surrounding values. If the missing value was at H00 or at H10, it could not undergo this type of imputation so the corresponding proteins were discarded. A sub-set of 3268 proteins was monitored in the time course experiment. The significant temporal dynamics were defined with the time course package in R Bioconductor, which uses a multivariate empirical Bayes model to rank proteins (Tai, 2007). Replicated time course data can be compared allowing for variability both within and between time points. Microarray and proteomics data present several thousands of candidates for a minimal number of time points and of replicates. These limitations are taken into account by this model, and Tai and Speed call this “moderation.” The mb.long method was used to calculate moderated Hotelling T^2 statistic, specifying a one-dimensional method (method = “1D”), where significant proteins change over meiosis time. The null hypothesis is that the protein temporal profile equal to 0. A threshold of 1 (in $\log_2$) as the minimal protein expression change between the higher and the lower time point was then applied. A high confidence dataset of 880 proteins was generated using these filtering rules although some moderate or transient protein changes may have been filtered out.

Protein expression changes were clustered following 6 different pre-defined temporal profiles. Therefore, proteins were matched against each temporal profile using the summed Euclidean distance for all time points. Proteins were then assigned to the cluster with the minimal Euclidian distance. The clustering was done for each replicate separately. A protein was definitively assigned to a profile cluster if the same matching behavior was observed in at least 2 biological replicates.

GO term enrichment was performed using the STRING database (Szklarczyk et al., 2015).

Correlation analysis

Correlation analyses were performed with home-made programs in the Python programming language (Python Software Foundation, https://www.python.org/) using numpy (https://www.numpy.org/), pandas (https://www.pandas.pydata.org/) and Scikit-learn (Pedregosa et al., 2011) libraries and Jupyter notebook (Kluyver et al., 2016).

Biological replicates were evaluated by calculating the Pearson correlation coefficients for each protein and each time point between protein levels in $\log_2$ of two given biological experiments. Mean values are plotted on a heatmap diagram.

Temporal dynamics of protein expression are evaluated by calculating the Pearson correlation coefficients for all possible pairs of time points on protein levels in $\log_2$ for each replicate independently. Mean values are plotted on a heatmap diagram.

mRNA data were downloaded from (Mata et al., 2002) and ribosome occupied mRNA data from (Duncan and Mata, 2014); referred to as “ribosome” hereafter). Genes for which protein and mRNA or ribosome levels were quantified were retained: a subset of 3077 genes for the mRNA/protein dataset and of 3233 genes for the ribosome/protein dataset. Likewise only common time points between the protein and mRNA or ribosome datasets were used.

Pearson correlation coefficients between mRNA (or ribosome) and mean protein levels expressed in $\log_2$ (arithmetic mean) were calculated and values are plotted on a histogram for the entire dataset, as well as for each protein cluster. The mean and the median Pearson correlation coefficients were calculated.

To distinguish between correlated and non-correlated pairs, the relative distances between normalized z-score mRNA (or ribosome) and normalized z-score mean protein levels for each time point were calculated ([RNA]Ti – [protein]Ti). For a good correlation, the relative distance will be close to 0. A positive relative distance indicates that the RNA levels are higher relative to protein levels and vice versa.

Clustering was performed on the relative distances by k-means (MiniBatchKMeans; (Sculley, 2010). In the case of the mRNA/protein dataset, k = 3 gave the most consistent result: group 1 (N = 1316) is an ensemble of correlated mRNA/protein pairs, group 2 (N = 861) contains uncorrelated pairs with a decrease in relative protein levels and increase in relative mRNA levels during meiosis, and group 3 (N = 900) is composed of uncorrelated pairs with an increase in relative protein levels and a decrease in relative mRNA levels during meiosis. Lowering the number of clusters (k = 2) removes group1, whereas increasing the number of clusters (k = 4) splits group1 into two groups, based on a difference at time point T5. In the case of the ribosome/protein dataset, k = 2 gave the most consistent result: group A (N = 1829) contains the correlated pairs whereas group B (N = 1404) is composed of uncorrelated pairs with an increase in relative protein levels and a decrease in relative mRNA levels during meiosis. Increasing the number of clusters (k = 3) splits group A into two groups. However, a cluster containing uncorrelated pairs with a decrease in relative protein levels and increase in relative mRNA levels during meiosis did not emerge.

The Pearson correlation coefficients for each mRNA (or ribosome occupied mRNA)/protein pair in a given cluster is plotted on a distribution histogram. The mean and the median Pearson correlation coefficients are calculated. For each cluster, mRNA (or ribosome) and protein levels in z-score are plotted over time. The relative distance over time is represented on a violin plot to better illustrate the density of the data at different values; the bar represents the mean.

Genes showing a good ribosome/protein correlation (Pearson correlation coefficient > = 0.4) were retrieved and their distribution within the mRNA/protein groups analyzed. The data are plotted as number of genes per group in a bar plot.

S. cerevisiae genes containing an upstream AUG in micro-ORF and showing a poor mRNA/protein correlation (Pearson correlation coefficient < 0.4) were downloaded from (Cheng et al., 2018). *S.pombe* orthologs were identified based on the *S.pombe-S.cerevisiae* ortholog table (data from Table S12 of (Gunaratne et al., 2013): this dataset was called LUTI. Genes containing an AUG in their micro-ORF (Pombase) were identified for both all quantified proteins and LUTI categories (quantified proteins: 55.3% have an AUG; LUTI: 59.6% have an AUG). Pearson correlation coefficients were calculated and plotted on a density plot. The overall density plot with or without an upstream AUG was similar for both categories. Moreover, the number of genes with an upstream AUG showing a poor mRNA/protein correlation (Pearson correlation coefficient < 0.4) are not enriched compared to the whole population (quantified proteins: 56.5% have an AUG; LUTI: 61.6% have an AUG).

Protein analysis

Ribosome biogenesis (GO:0042254) and proteolysis (GO:0006508) proteins present in the significantly varying proteins were expressed in percent per cluster and plotted on a bar plot.

Meiotically upregulated genes (mug) were downloaded from (Martín-Castellanos et al., 2005) and Rep1p, Mei4p and Atf21p/Atf22p target genes were downloaded from (Mata et al., 2007). Two plots were produced: First, for each subset, Pearson correlation coefficients between mRNA and mean protein levels expressed in $\log_2$ (arithmetic mean) were calculated and values were plotted on a histogram. The mean and the median Pearson correlation coefficients were also calculated. For the second plot, significantly varying proteins present in these subsets were retrieved and expressed in percent per cluster on a bar plot.

Western blot quantification

For the quantification of the intensity of the proteins during the meiotic cycle, primary antibody titrations were performed to assure detection in the linear range. The dilutions used were as follow: GFP antibody (1:500), 9E10 (1:500), 12CA5 (1:500), actin antibody (1:200), and cdc13 antibody (1:500). Quantification was performed using ImageJ software. Rectangles of equal size were drawn over the protein lanes and the intensity of the signal plotted on a histogram. Intensities were defined as the area below the peaks. Values were then corrected by normalizing to the values obtained using the actin monoclonal antibody (internal control), and the standardized values (z-score) were plotted with the appropriate timescale shift to correct for different meiotic induction times in the different strains.

DATA AND SOFTWARE AVAILABILITY

All raw data and MaxQuant output files can be accessed via the PRIDE partner repository (http://www.ebi.ac.uk/pride/archive/) with the accession number PRIDE: PXD101438.

Figures, tables and scripts are available at Mendeley Data (https://doi.org/10.17632/wr4xddybvg.1)